DOI: 10.1161/CIRCULATIONAHA.115.016270

Inducing Persistent Flow Disturbances Accelerates Atherogenesis and Promotes Thin Cap Fibroatheroma Development in *D374Y*-PCSK9 Hypercholesterolemic Minipigs

Running title: *Pedrigi et al.; Inducing low shear stress causes TCFA formation*

Ryan M. Pedrigi, PhD[1]*; Christian Bo Poulsen, MD[2,3]*; Vikram V. Mehta, PhD[1]; Niels Ramsing Holm, MD[2,3]; Nilesh Pareek, MB, BChir, MA[4]; Anouk L. Post, MSc[1]; Ismail Dogu Kilic, MD[4]; Winston A.S. Banya, MSc[4]; Gianni Dall'Ara, MD[4]; Alessio Mattesini, MD[4]; Martin M. Bjørklund, MD[2,3]; Niels P. Andersen, MD[2,3]; Anna K. Grøndal, MD[2,3]; Enrico Petretto, PhD[5]; Nicolas Foin, PhD[6]; Justin E. Davies, MBBS, PhD[7]; Carlo Di Mario, MD, PhD[4,7,8]; Jacob Fog Bentzon, MD, PhD[2,3]; Hans Erik Bøtker, MD, PhD[3]; Erling Falk, MD, PhD[2,3]; Rob Krams, MD, PhD[1]; Ranil de Silva, MBBS, PhD[4,7,8]

[1]Dept of Bioengineering, Imperial College London, United Kingdom; [2]Institute of Clinical Medicine, Aarhus University Hospital, Aarhus, Denmark; [3]Dept of Cardiology, Aarhus University Hospital, Aarhus, Denmark; [4]NIHR Cardiovascular Biomedical Research Unit, Royal Brompton and Harefield NHS Foundation Trust, London, United Kingdom; [5]Graduate Medical School, Duke-National University of Singapore, Singapore; [6]National Heart Centre, NHRIS, Singapore; [7]National Heart and Lung Institute, Imperial College London, United Kingdom; [8]Institute of Cardiovascular Medicine and Science, Royal Brompton and Harefield NHS Foundation Trust, London, United Kingdom

*Joint first authors who contributed equally

Address for Correspondence:
Ranil de Silva, MBBS, PhD
National Heart and Lung Institute (Brompton Campus)
Imperial College London and NIHR Cardiovascular Biomedical Research Unit
Royal Brompton and Harefield NHS Foundation Trust
Level 2 Chelsea Wing, Sydney Street
London SW3 6NP, United Kingdom
Tel: +442073518626
Fax: +442073518629
E-mail: r.desilva@imperial.ac.uk

Journal Subject Codes: Atherosclerosis:[134] Pathophysiology, Atherosclerosis:[150] Imaging, Atherosclerosis:[87] Coronary circulation, Basic science research:[130] Animal models of human disease, Diagnostic testing:[29] Coronary imaging: angiography/ultrasound/Doppler/CC

DOI: 10.1161/CIRCULATIONAHA.115.016270

Abstract

Background—Although disturbed flow is thought to play a central role in the development of advanced coronary atherosclerotic plaques, no causal relationship has been established. We evaluated whether inducing disturbed flow would cause the development of advanced coronary plaques, including thin cap fibroatheroma (TCFA).

Methods and Results—*D374Y*-PCSK9 hypercholesterolemic minipigs (*N*=5) were instrumented with an intracoronary shear-modifying stent (SMS). Frequency-domain optical coherence tomography was obtained at baseline, immediately post-stent, 19, and 34 weeks and used to compute shear stress metrics of disturbed flow. At 34 weeks, plaque type was assessed within serially-collected histological sections and co-registered to the distribution of each shear metric. The SMS caused a flow-limiting stenosis and blood flow exiting the SMS caused regions of increased shear stress on the outer curvature and large regions of low and multidirectional shear stress on the inner curvature of the vessel. As a result, plaque burden was ~3-fold higher downstream of the SMS compared to both upstream of the SMS and in the control artery (p<0.001). Advanced plaques were also primarily observed downstream of the SMS, in locations initially exposed to both low (p<0.002) and multidirectional (p<0.002) shear stress. TCFA regions demonstrated significantly lower shear stress that persisted over the duration of the study compared to other plaque types (p<0.005).

Conclusions—These data support a causal role for lowered and multidirectional shear stress in the initiation of advanced coronary atherosclerotic plaques. Persistently lowered shear stress appears to be the principal flow disturbance needed for the formation of TCFA.

Key words: atherogenesis, shear stress, thin cap fibroatheroma, optical coherence tomography

DOI: 10.1161/CIRCULATIONAHA.115.016270

Introduction

Coronary heart disease (CHD) is projected to remain the worldwide leading cause of death until 2030[1]. CHD is a major cause of morbidity and reduced quality of life with enormous economic consequences[2, 3]. Atherosclerosis, a multifocal lipid-driven inflammatory process, is the principal underlying pathology in patients with CHD, which commonly presents clinically with symptoms secondary to luminal narrowing of an epicardial coronary artery or an acute coronary syndrome (ACS). The latter is a major cause of CHD death and most commonly results from rupture at the site of a thin cap fibroatheroma (TCFA) leading to coronary thrombosis[4].

The precise environmental cues that lead plaques towards an advanced and high risk phenotype are not yet fully elucidated, but disturbed blood flow is thought to play a central role in both lesion initiation and progression[5]. Disturbed flow is most frequently quantified by metrics of shear stress, which is the frictional force imposed by blood flowing over the endothelial surface, and association between these metrics and coronary atherosclerotic lesion stage have been demonstrated *in vivo* in both animal models[6-9] and patients[10, 11]. However, few studies have investigated the impact of prevalent shear conditions on longitudinal development of advanced coronary plaques, wherein they report discrepant results. Previous experimental studies[6-8, 12] have reported TCFA development in arterial segments with persistently low time-averaged wall shear stress (WSS) in diabetic hypercholesterolemic pigs. By contrast, clinical studies[11] suggested that regions of high WSS were associated with development of features of plaque vulnerability. This work also showed an association between low WSS and regional plaque progression, consistent with the findings of the PREDICTION trial[10]. While informative, these important studies do not confirm a causal role for metrics of disturbed WSS in inducing the formation and progression of advanced coronary plaques.

In the current study, we hypothesized that: (i) inducing disturbed blood flow initiates development of advanced coronary plaque types, including TCFA, and (ii) different longitudinal patterns of low, multidirectional, and high WSS metrics determine plaque morphology. To test these hypotheses, we developed a stenotic shear modifying stent (SMS)[13] that could be placed percutaneously to induce regions of persistent blood flow perturbations within the coronary arteries of *D374Y*-PCSK9 hypercholesterolemic transgenic minipigs[14]. Our results provide evidence for a causal role of disturbed flow in the development of advanced coronary plaques and extend our previous work demonstrating that inducing disturbed blood flow in a carotid artery of hypercholesterolemic mice[15, 16] causes the development of TCFA-like plaques.

Methods

Detailed methods are available in the online supplement and the study protocol is summarised in **Supplemental Figure 1**. All animal experiments were performed in accordance with the ethical and welfare regulations of the University of Aarhus and approved by the Danish Animal Experiments Inspectorate. Briefly, SMS were implanted into either the left anterior descending (LAD) or left circumflex (LCx) arteries of hypercholesterolemic *D374Y* PCSK9 transgenic minipigs (*N*=6), with the unstented artery serving as a control[14]. Serial intracoronary frequency domain optical coherence tomography (FD-OCT) and Doppler flow velocity measurements were obtained at 0 (baseline), 0+ (immediately post-stent), 19, and 34 weeks. From these data, the 3-D geometry of each artery was reconstructed and computational fluid dynamics (CFD) was performed to compute established and custom WSS metrics of disturbed flow. To correlate computed WSS metrics to plaque morphology, vessel segments were excised proximal and distal to the SMS in the instrumented artery and in a comparable region of the uninstrumented control

artery at the final study time point. The segments were serially sectioned and alternating sections were stained with hematoxylin and eosin (H&E), picrosirius red (collagen), and muramidase (pan macrophage). Stained histological sections from each pig were imaged, contoured manually, and accurately co-registered to the corresponding segments of the *in vivo* 3-D reconstructed arteries of that pig over all time points, to evaluate on a local basis (3.6° circumferentially and ~105 □m axially) the time-course of change in magnitude of each WSS metric within each plaque type. Plaques were independently classified by expert histopathologists, who were blinded to CFD results, as TCFA, fibrous cap atheroma (FCA), pathological intimal thickening (PIT), xanthoma (XA), intimal thickening (IT), or normal vessel wall (NOR). A color coding system was used to segment plaque type continuously around the circumference of each H&E-stained section (**Supplemental Figure 2**). The primary readout was the mean of each WSS metric within each of the plaque types identified in each histological section, averaged over all sections containing that plaque type across all pigs. The accuracy of this workflow was confirmed in a formal error analysis (see Supplemental Methods).

Statistical Analysis

Variables (stenosis area, blood velocity and total cholesterol) are reported as mean±SD. Some variables (WSS metrics of disturbed flow and metrics of plaque size) were log-transformed and reported as geometric mean with 95% confidence interval (GM [95% CI]). All statistical analyses were performed using a linear mixed-effects model to compare continuous dependent variables and various independent categorical variables, including: plaque type or group (fixed effect), time (fixed effect), and subject (random effect due to repeated measures of multiple histological sections within each pig). Comparisons between normally distributed variables are expressed as an arithmetic mean difference with 95% confidence interval (AMD [95%CI]) and

log-transformed distributed variables are expressed as a geometric mean ratio with 95% confidence interval (GMR [95%CI]). Both outputs come directly from the mixed model with an associated *p*-value. All *p*-values generated from the linear mixed-effect model and reported in the manuscript have been systematically Bonferroni corrected by multiplying each *p*-value by the appropriate number of comparisons. Statistical significance was based on these corrected *p*-values being less than 0.05. All statistical analyses were performed in Stata version 13 (StataCorp, College Station, TX, USA).

Results

One pig died due to acute stent thrombosis immediately after SMS implantation. Of the remaining 5 pigs, 4 animals completed the entire study protocol, with one animal dying after developing stent thrombosis following completion of intracoronary imaging at the 19 week time point. A total of 5957 FD-OCT frames were contoured manually to allow reconstruction and CFD modelling for calculation of WSS in 38 vessels comprised of both instrumented and control arteries over all time points in 5 pigs. Histology sections were co-registered to the corresponding 3-D reconstructed arteries. Local plaque type was manually segmented in H&E stained sections (*N*=538). Regional overlaps between these histological measures and WSS metrics of disturbed flow were quantified.

SMS induced atherogenesis and advanced plaque development

We observed accelerated atherosclerosis resulting from SMS placement. Compared to control regions, the segment downstream of the SMS had moderately increased external elastic lamina (EEL) area (GM 2.1 [2.0, 2.2] mm^2 vs 1.4 [1.3, 1.5] mm^2 and GMR 1.6 [1.4, 1.8]; $p<0.001$) and large increases in plaque area (GM 1.3 [1.1, 1.5] mm^2 vs 0.2 [0.2, 0.3] mm^2 and GMR 6.0 [4.7,

8.0]; $p<0.001$). The segment upstream of the SMS had similar increases in EEL area (GM 2.1 [1.9, 2.3] mm^2 vs 1.4 [1.3, 1.5] mm^2 and GMR 1.5 [1.3, 1.7]; $p<0.001$) but plaque area only increased modestly (GM 0.3 [0.3, 0.4] mm^2 vs 0.2 [0.2, 0.3] mm^2 and GMR 1.5 [1.1, 2.0]; $p=0.012$), which was significantly less than in the downstream segment (GMR 4.0 [3.3, 5.0] in downstream versus upstream plaque area; $p<0.001$). Strikingly, plaque burden was ~3-fold higher in the segment downstream of the SMS compared to both the SMS upstream (GMR 3.4 [2.9, 4.1]; $p<0.001$) and control artery segments (GMR 3.5 [2.8, 4.4]; $p<0.001$; **Figure 1A**).

Sections from the segment downstream of the SMS exhibited plaques at varying stages of advancement (**Figure 1B**), including NOR (34%), IT (20%), XA (17%), PIT (22%), FCA (4%) and TCFA (3%). FCA and TCFA lesions contained a large necrotic core, macrophage infiltration, and a fibrous cap (≤65 μm for TCFA) with newly deposited collagen, similar to human lesions (**Figure 1B**). The following plaque types developed in the region upstream of the SMS: NOR (36%), IT (29%), XA (10%), PIT (20%), and FCA (5%). No TCFA was observed. Sections from segments of the uninstrumented artery exhibited NOR (41%), IT (30%), XA (5%), and PIT (24%), but no FCA or TCFA were observed (**Supplemental Figure 3**).

SMS implantation caused persistent wall shear stress perturbations

The arithmetic mean initial maximum areal stenosis created by the SMS was 62.6±7.0% ($N=5$). There was a progressive increase in stenosis severity to 83.9±3.1% at 34 weeks (AMD 20.9 [14.5, 27.4] at 34 weeks versus immediately post-SMS; $p<0.001$) due to neo-intimal hyperplasia within the SMS (**Figure 2A, 2B**). The stenosis resulted in a reduction of mean blood velocity at the inlet of the instrumented vessel from 147.8±41.0 at baseline to 90.7±19.2 mm/s at 34 weeks (AMD -57.1 [-93.7, -20.3] mm/s at 34 weeks versus baseline; $p=0.018$). The change in blood velocity in the control vessel over time was not statistically significant ($p=0.55$; **Figure 2C**). The

reduced blood velocity caused a concomitant reduction in WSS in the instrumented vessel (**Figure 2D**). Notably, in the region downstream of the SMS, the accelerated blood flow exiting the SMS was directed towards the outer curvature of the vessel in a concentrated stream, causing regions of markedly increased flow localized to the outer curvature. This high kinetic energy in the concentrated stream induced flow separation and vortex formation, causing large regions with low and multidirectional flow on the inner curvature (**Figure 2E**). WSS metrics with the largest positive change from baseline values over time were the low shear index (LSI), indicating regions with lowered WSS; high shear index (HSI), indicating regions with increased WSS; and a variant of the transverse wall shear stress (tSS; **Figure 2D**), indicating multidirectional flow. We therefore focused on these metrics for the remainder of the study.

Advanced plaques were initiated by low and multidirectional wall shear stress

After observing that placement of the SMS increased LSI, HSI, and tSS, we next evaluated whether any of these metrics of disturbed flow preferentially co-localized to regions of particular plaque types immediately after SMS implantation (t=0+) to explore the initiating stimulus for those plaques. Plaques were initially grouped as advanced lesions (TCFA, FCA, and PIT), early lesions (XA and IT), or normal vessel wall (NOR) in the segments upstream and downstream of the SMS, as well as the uninstrumented control artery of all pigs. In all histological sections, we quantified the geometric mean of each WSS metric within each plaque group at t=0+ (**Figure 3**). LSI within advanced lesions located in the downstream segment (N=125 sections) was significantly higher compared to those in the upstream (GMR 29.3 [20.7, 41.6]; N=86; p<0.002) and control segments (GMR 17.9 [10.9, 29.3]; N=33; p<0.002). LSI, which is a measure that increases in value as WSS reduces, was also significantly greater in advanced compared to early lesions (GMR 5.5 [4.1, 7.3]; p<0.002) and normal vessel wall (GMR 6.9 [5.2, 9.1]; p<0.002) in

the instrumented downstream segment (**Figure 3A**). By comparison HSI, which is a measure that increases in value as WSS increases, exhibited a reverse pattern in the downstream segment with reduced values in advanced lesions (except FCA at 19 weeks, see below) that were significantly lower compared to early lesions (GMR 0.62 [0.51, 0.76]; $p<0.002$) and normal vessel (GMR 0.46 [0.38, 0.56]; $p<0.002$; **Figure 3B**). Similar to LSI in the downstream segment, tSS had larger values in advanced lesions compared to both early lesions (GMR 1.7 [1.5, 1.9]; $p<0.002$) and normal vessel (GMR 1.8 [1.6, 2.0]; $p<0.002$). Overall, the striking co-localization of advanced lesions to regions of lowered WSS (LSI) and multidirectional WSS (tSS) within the downstream segment, where plaque burden was ~3-fold higher compared to other regions, suggests that both patterns of disturbed flow contributed to their initiation.

The time course and magnitude of disturbed wall shear stress determined final plaque type

Next, we determined whether each plaque type experienced a different time course of disturbed flow in the segment downstream of the SMS (**Figure 4**). TCFA, FCA, and PIT were observed in 2/5, 3/5 and 5/5 animals, respectively. Over all post-instrumentation times, TCFA regions demonstrated higher LSI values (**Figure 5A**) compared to FCA (GMR 1.8 [1.3, 2.5]; $p<0.005$) and PIT (GMR 1.4 [1.1, 1.9]; $p=0.25$), although only the comparison with FCA was statistically significant. LSI in TCFA was also significantly higher compared to XA (GMR 1.94 [1.47, 2.56], $p<0.005$), IT (GMR 2.75 [2.10, 3.58]; $p<0.005$), and normal vessel wall (GMR 2.66 [2.05, 3.46]; $p<0.005$). In addition, LSI values were of greater magnitude in PIT compared with values in XA (GMR 1.4 [1.2, 1.6]; $p<0.005$), IT (GMR 1.9 [1.7, 2.2]; $p<0.005$), and normal vessel wall (GMR 1.9 [1.7, 2.1]; $p<0.005$). LSI was also higher in FCA compared to IT (GMR 1.5 [1.2, 1.9]; $p<0.005$) and normal wall (GMR 1.5 [1.2, 1.9]; $p<0.005$), but not XA (1.1 [0.9, 1.4]; $p=0.90$). Interestingly, FCA was also the only advanced plaque with increased HSI (**Figure 5B**), wherein

at 19 weeks FCA was increased compared to PIT (GMR 3.2 [1.8, 5.6]; $p<0.005$) and TCFA (GMR 2.5 [0.9, 5.6]; $p=0.79$), although the latter comparison was not significant. Finally, analysis of tSS (**Figure 5C**) over all post-instrumentation times was not statistically higher between any of the advanced plaque types and only TCFA and PIT showed any statistically higher values of tSS, when compared to IT (GMR 1.4 [1.2, 1.7] and 1.3 [1.1, 1.4], respectively; $p<0.005$) and normal vessel wall (GMR 1.4 [1.2, 1.7] and 1.3 [1.2, 1.4], respectively; $p<0.005$; **Figure 5C**).

Discussion

Previous studies have reported the association between naturally-occurring disturbed blood flow and the development of atherosclerotic lesions[6-11]. These investigations have supported the hypothesis that persistent, low WSS may initiate and progress the development of high risk plaque features, but do not prove its causal role. In the current study, we imposed a persistent perturbation of local WSS by implantation of a SMS. The main findings of our study were, first, that SMS implantation induced a heterogeneous pattern of flow disturbance that caused accelerated atherogenesis and formation of advanced plaque types in the coronary arteries of *D374Y*-PCSK9 hypercholesterolemic minipigs. Second, we observed that the majority of advanced plaques were located in the segment downstream of the SMS (**Figure 1**) within regions of initially lowered WSS (quantified by LSI) and also multidirectional WSS (quantified by tSS; **Figure 3**). In contrast, the upstream SMS and control artery segments exhibited little overlap between WSS metrics of disturbed flow and any plaque type (**Supplemental Figure 4**). Third, we observed that compared to other advanced plaque types, TCFA developed in those locations downstream of the SMS exposed to the largest and most persistent reduction in WSS over the

duration of the study (**Figure 5A**), consistent with previous observations[8]. Finally, FCA developed in locations subjected to greater degrees of high WSS (quantified by HSI), particularly at 19 weeks (**Figure 5B**), which supports the hypothesis that high WSS may promote a stable plaque phenotype. Collectively, these findings demonstrate a causal role for disturbed flow in the formation of advanced plaques, including TCFA, within coronary arteries.

Building on initial studies that suggested a pro-atherogenic role for low and oscillatory WSS[17, 18], we previously reported that placing a constrictive, external cuff to perturb blood flow in the carotid artery of Apo-E knockout mice led to the formation of TCFA upstream and a stable plaque downstream of this device. This approach provided the first evidence for a causal role of disturbed blood flow in vulnerable and stable plaque formation[16]. However, their small size and different cardiovascular physiology imposes limitations on the study of atherosclerosis progression and predilection sites as it relates to man. Furthermore, Reynolds and Dean numbers scale with size and are significantly lower in rodent models as compared with values in man[19]. Recent data also suggest limitations of murine models for studying acute inflammatory disease processes[20]. We were therefore motivated to overcome these limitations by studying the coronary arteries of a transgenic hyperlipidemic pig model which, in contrast to murine models, develops human-like advanced plaques[14]. Our results are consistent with previous observations that lowering WSS induces TCFA[15, 16]. We now demonstrate that in addition to co-localization with regions of early atherosclerotic lesion formation[21], multidirectional WSS may act synergistically with lowered WSS to initiate development of advanced coronary plaques including TCFA, which has not been reported previously. In addition, our observations that early exposure to raised WSS, quantified by HSI, significantly overlapped with formation of early plaque types (**Figure 3B**) and that exposure to high WSS was associated with the development

of FCA (**Figure 5B**), supports further investigation of the hypothesis that high WSS may be protective by inducing formation of stable plaque phenotypes.

The marked variation in plaque type observed in both the axial and circumferential directions of each instrumented vessel (**Figure 4**) motivated our novel approach to determine how temporal changes in WSS may influence final plaque morphology on a local, high-resolution scale. This type of analysis is important as plaque rupture is likely determined by variations in the biomechanical properties, and possibly endothelial cell mechanobiology, on this scale[22]. This approach was enabled by using FD-OCT rather than intravascular ultrasound (IVUS) for 3-D reconstruction of the vessel lumen and its curvature. We performed a detailed error propagation analysis that confirmed an error of less than 10% for computed WSS despite using a commercial FD-OCT system that could not provide ECG-gated acquisitions. In addition, we performed a detailed error analysis of the 3-D histology approach developed for co-registering WSS metrics from CFD to histological data, which demonstrated a circumferential error of 265 μm and axial error of 340 μm that represents a significant improvement to previous reports from both others[6-8, 12, 23, 24] and ourselves[25-29]. Importantly, this 3-D histology error analysis included assessment of the reproducibility of identification of the same vessel segment of interest from the FD-OCT images through time. Therefore, it accounts for small changes in vessel size that may occur over time due to remodelling or acquisition of the FD-OCT at different average positions within the cardiac cycle (see Supplemental Methods).

Our data show that development of advanced lesions in the SMS treated artery directly resulted from induced changes in local blood flow. Two new metrics were developed to quantify those changes relative to the instrumented vessel at baseline (i.e., before SMS placement) over a continuous range, namely the LSI and HSI. These metrics require no *a priori* assumption of a

threshold value of WSS for determining non-normal WSS magnitudes and are applicable to the study of animals of different sizes and humans. This approach may facilitate evaluation of changes in WSS over time by overcoming potential issues arising from using a global threshold for defining low and high WSS, as previously reported in the literature[6-8, 23, 30-32]. Interestingly, the geometric mean of the absolute values of WSS within regions of LSI was 0.7 [0.6, 0.8] Pa (**Supplemental Figure 5**), which is lower than the binary threshold values of 1 to 1.2 Pa reported previously[6-8, 23, 30-32].

The finding that low and multidirectional flow accelerated the initiation and development of all advanced plaque types is consistent with previous experimental data demonstrating that such flow disturbances promote a pro-atherogenic endothelial cell type, which is characterized by: increased expression of pro-inflammatory adhesion molecules[33, 34], impaired nitric oxide production[35], increased production of reactive oxygen species, augmented permeability to LDL[36] and enhanced attraction and adhesion of monocytes. Furthermore, studies in hyperlipidemic mice[37], rabbits[38], pigs[12], and humans[10] consistently demonstrate that atherosclerotic lesions preferentially occur in regions with natural low and multidirectional WSS conditions, including curved vessel segments and bifurcations[39].

We studied *D374Y*-PCSK9 transgenic hypercholesterolemic Yucatan minipigs which have growth curves that suit long term serial invasive follow-up studies and exhibit chronically elevated cholesterol when fed a cholate-free high fat high cholesterol diet (HFHC), resulting from a gain of function mutation in the proprotein convertase subtilisin/kexin type 9 gene resulting in impaired LDL cholesterol clearance. When fed the HFHC diet used in this study, these animals typically achieve a total cholesterol of ~20 mmol/L (~773 mg/dl) and LDL cholesterol of ~11 mmol/L (~425 mg/dl)[14], which is similar to the cholesterol levels of animals

in the current study (**Supplemental Figure 6**).

Study limitations

Several limitations of this study should be considered. First, a small cohort of 5 pigs were studied and human-like fibroatheromata developed in only 3/5 animals, including TCFA in 2/5 animals. Even with this sample size, the high-resolution analysis provided sufficient power to allow identification of statistically significant associations between WSS metrics and final plaque morphology. However, further studies in a larger cohort are needed to provide sufficient sample size to assess the relative magnitude, sensitivity, and specificity of LSI, HSI, and tSS, or their combination, for precise prediction of the development of each advanced plaque type. Second, the temporal evolution of WSS metrics could be related to plaque morphology only at the final time point, when the animals were euthanized for histology. Further work is needed to evaluate the time course of development of each advanced plaque. Extending the duration of follow-up and HFHC diet with further histological evaluation of the proximal portion of the coronary arteries is also needed to enable more detailed comparison of the determinants of advanced plaque development in the uninstrumented and SMS-treated arteries. Our results suggest the utility of this model for longitudinal studies of the development of advanced human-like plaques, including TCFA, especially as advanced plaques develop at a predictable location within the coronary artery tree in a practical timeframe. Finally, in the current study, we principally considered the effect of induced local flow disturbance through placement of the SMS. While this intervention may induce an altered arterial remodeling response compared to that induced by naturally-occurring flow disturbances, we suggest that this approach enables direct testing of the causal role of different patterns of flow disturbances on advanced coronary atherosclerotic lesion development and thus complements natural history studies.

Conclusions

We have established a novel model of accelerated atherogenesis and formation of advanced human-like atherosclerotic plaques, including TCFA. This model combined with FD-OCT derived CFD and 3-D histology provides a new means of studying the biomechanics and mechanobiology of human-like advanced coronary plaques. Our results demonstrate a causal role for lowered and multidirectional WSS within the coronaries as determinants of final plaque type. Persistently lowered WSS appears to be the principal hemodynamic disturbance needed for the formation of TCFA. Further investigation to specify the relative contributions of persistently decreased, increased, and altered multidirectional shear stress on the development of each of the different advanced coronary atherosclerotic plaque types is warranted.

Acknowledgments: We thank Zahra Nasr, Lisa Maria Røge, and Dorte Qualmann for technical assistance.

Funding Sources: This work was supported by the NIHR Cardiovascular Biomedical Research Unit, Royal Brompton and Harefield NHS Foundation Trust (RdS); BHF Program Grant (RG11/13/29055); Helga and Peter Kornings Fund and Aarhus University.

Conflict of Interest Disclosures: NRH has received institutional research grants and speaker fees from St. Jude Medical and Terumo.

References:

1. Mathers CD, Loncar D. Projections of global mortality and burden of disease from 2002 to 2030. *PLoS Med*. 2006;3:e442.

2. Go AS, Mozaffarian D, Roger VL, Benjamin EJ, Berry JD, Borden WB, Bravata DM, Dai S, Ford ES, Fox CS, Franco S, Fullerton HJ, Gillespie C, Hailpern SM, Heit JA, Howard VJ, Huffman MD, Kissela BM, Kittner SJ, Lackland DT, Lichtman JH, Lisabeth LD, Magid D, Marcus GM, Marelli A, Matchar DB, McGuire DK, Mohler ER, Moy CS, Mussolino ME, Nichol G, Paynter NP, Schreiner PJ, Sorlie PD, Stein J, Turan TN, Virani SS, Wong ND, Woo

D, Turner MB, American Heart Association Statistics C, Stroke Statistics S. Heart disease and stroke statistics--2013 update: A report from the american heart association. *Circulation*. 2013;127:e6-e245.

3. Leal J, Luengo-Fernandez R, Gray A, Petersen S, Rayner M. Economic burden of cardiovascular diseases in the enlarged european union. *Eur Heart J*. 2006;27:1610-1619.

4. Falk E, Nakano M, Bentzon JF, Finn AV, Virmani R. Update on acute coronary syndromes: The pathologists' view. *Eur Heart J*. 2013;34:719-728.

5. Wentzel JJ, Chatzizisis YS, Gijsen FJ, Giannoglou GD, Feldman CL, Stone PH. Endothelial shear stress in the evolution of coronary atherosclerotic plaque and vascular remodelling: Current understanding and remaining questions. *Cardiovasc Res*. 2012;96:234-243.

6. Chatzizisis YS, Baker AB, Sukhova GK, Koskinas KC, Papafaklis MI, Beigel R, Jonas M, Coskun AU, Stone BV, Maynard C, Shi GP, Libby P, Feldman CL, Edelman ER, Stone PH. Augmented expression and activity of extracellular matrix-degrading enzymes in regions of low endothelial shear stress colocalize with coronary atheromata with thin fibrous caps in pigs. *Circulation*. 2011;123:621-630.

7. Koskinas KC, Feldman CL, Chatzizisis YS, Coskun AU, Jonas M, Maynard C, Baker AB, Papafaklis MI, Edelman ER, Stone PH. Natural history of experimental coronary atherosclerosis and vascular remodeling in relation to endothelial shear stress: A serial, in vivo intravascular ultrasound study. *Circulation*. 2010;121:2092-2101.

8. Koskinas KC, Sukhova GK, Baker AB, Papafaklis MI, Chatzizisis YS, Coskun AU, Quillard T, Jonas M, Maynard C, Antoniadis AP, Shi GP, Libby P, Edelman ER, Feldman CL, Stone PH. Thin-capped atheromata with reduced collagen content in pigs develop in coronary arterial regions exposed to persistently low endothelial shear stress. *Arterioscler Thromb Vasc Biol*. 2013;33:1494-1504.

9. Thim T, Hagensen MK, Horlyck A, Kim WY, Niemann AK, Thrysoe SA, Drouet L, Paaske WP, Botker HE, Falk E. Wall shear stress and local plaque development in stenosed carotid arteries of hypercholesterolemic minipigs. *J Cardiovasc Dis Res*. 2012;3:76-83.

10. Stone PH, Saito S, Takahashi S, Makita Y, Nakamura S, Kawasaki T, Takahashi A, Katsuki T, Nakamura S, Namiki A, Hirohata A, Matsumura T, Yamazaki S, Yokoi H, Tanaka S, Otsuji S, Yoshimachi F, Honye J, Harwood D, Reitman M, Coskun AU, Papafaklis MI, Feldman CL, Investigators P. Prediction of progression of coronary artery disease and clinical outcomes using vascular profiling of endothelial shear stress and arterial plaque characteristics: The prediction study. *Circulation*. 2012;126:172-181.

11. Samady H, Eshtehardi P, McDaniel MC, Suo J, Dhawan SS, Maynard C, Timmins LH, Quyyumi AA, Giddens DP. Coronary artery wall shear stress is associated with progression and transformation of atherosclerotic plaque and arterial remodeling in patients with coronary artery disease. *Circulation*. 2011;124:779-788.

12. Chatzizisis YS, Jonas M, Coskun AU, Beigel R, Stone BV, Maynard C, Gerrity RG, Daley W, Rogers C, Edelman ER, Feldman CL, Stone PH. Prediction of the localization of high-risk coronary atherosclerotic plaques on the basis of low endothelial shear stress: An intravascular ultrasound and histopathology natural history study. *Circulation*. 2008;117:993-1002.

13. Foin N, Sen S, Petraco R, Nijjer S, Torii R, Kousera C, Broyd C, Mehta V, Xu Y, Mayet J, Hughes A, Di Mario C, Krams R, Francis D, Davies J. Method for percutaneously introducing, and removing, anatomical stenosis of predetermined severity in vivo: The "stenotic stent". *J Cardiovasc Transl Res*. 2013;6:640-648.

14. Al-Mashhadi RH, Sorensen CB, Kragh PM, Christoffersen C, Mortensen MB, Tolbod LP, Thim T, Du Y, Li J, Liu Y, Moldt B, Schmidt M, Vajta G, Larsen T, Purup S, Bolund L, Nielsen LB, Callesen H, Falk E, Mikkelsen JG, Bentzon JF. Familial hypercholesterolemia and atherosclerosis in cloned minipigs created by DNA transposition of a human pcsk9 gain-of-function mutant. *Sci Transl Med*. 2013;5:166ra161.

15. Cheng C, Tempel D, van Haperen R, de Boer HC, Segers D, Huisman M, van Zonneveld AJ, Leenen PJ, van der Steen A, Serruys PW, de Crom R, Krams R. Shear stress-induced changes in atherosclerotic plaque composition are modulated by chemokines. *J Clin Invest*. 2007;117:616-626.

16. Cheng C, Tempel D, van Haperen R, van der Baan A, Grosveld F, Daemen MJ, Krams R, de Crom R. Atherosclerotic lesion size and vulnerability are determined by patterns of fluid shear stress. *Circulation*. 2006;113:2744-2753.

17. Pedersen EM, Oyre S, Agerbaek M, Kristensen IB, Ringgaard S, Boesiger P, Paaske WP. Distribution of early atherosclerotic lesions in the human abdominal aorta correlates with wall shear stresses measured in vivo. *Eur J Vasc Endovasc Surg*. 1999;18:328-333.

18. Davies PF, Polacek DC, Shi C, Helmke BP. The convergence of haemodynamics, genomics, and endothelial structure in studies of the focal origin of atherosclerosis. *Biorheology*. 2002;39:299-306.

19. de Crom R, Cheng C, Helderman F, Krams R. Large variations in absolute wall shear stress levels within one species and between species. *Atherosclerosis*. 2009;204:16-17; author reply 18-19.

20. Seok J, Warren HS, Cuenca AG, Mindrinos MN, Baker HV, Xu W, Richards DR, McDonald-Smith GP, Gao H, Hennessy L, Finnerty CC, Lopez CM, Honari S, Moore EE, Minei JP, Cuschieri J, Bankey PE, Johnson JL, Sperry J, Nathens AB, Billiar TR, West MA, Jeschke MG, Klein MB, Gamelli RL, Gibran NS, Brownstein BH, Miller-Graziano C, Calvano SE, Mason PH, Cobb JP, Rahme LG, Lowry SF, Maier RV, Moldawer LL, Herndon DN, Davis RW, Xiao W, Tompkins RG, Inflammation, Host Response to Injury LSCRP. Genomic responses in mouse models poorly mimic human inflammatory diseases. *Proc Natl Acad Sci U S A*. 2013;110:3507-3512.

21. del Alamo JC, Norwich GN, Li YS, Lasheras JC, Chien S. Anisotropic rheology and directional mechanotransduction in vascular endothelial cells. *Proc Natl Acad Sci U S A*. 2008;105:15411-15416.

22. Pedrigi RM, de Silva R, Bovens SM, Mehta VV, Petretto E, Krams R. Thin-cap fibroatheroma rupture is associated with a fine interplay of shear and wall stress. *Arterioscler Thromb Vasc Biol*. 2014;34:2224-2231.

23. Chatzizisis YS, Coskun AU, Jonas M, Edelman ER, Feldman CL, Stone PH. Role of endothelial shear stress in the natural history of coronary atherosclerosis and vascular remodeling: Molecular, cellular, and vascular behavior. *J Am Coll Cardiol*. 2007;49:2379-2393.

24. Wentzel JJ, Kloet J, Andhyiswara I, Oomen JA, Schuurbiers JC, de Smet BJ, Post MJ, de Kleijn D, Pasterkamp G, Borst C, Slager CJ, Krams R. Shear-stress and wall-stress regulation of vascular remodeling after balloon angioplasty: Effect of matrix metalloproteinase inhibition. *Circulation*. 2001;104:91-96.

25. Cheng C, Tempel D, Oostlander A, Helderman F, Gijsen F, Wentzel J, van Haperen R, Haitsma DB, Serruys PW, van der Steen AF, de Crom R, Krams R. Rapamycin modulates the enos vs. Shear stress relationship. *Cardiovasc Res*. 2008;78:123-129.

26. Cheng C, van Haperen R, de Waard M, van Damme LC, Tempel D, Hanemaaijer L, van Cappellen GW, Bos J, Slager CJ, Duncker DJ, van der Steen AF, de Crom R, Krams R. Shear stress affects the intracellular distribution of enos: Direct demonstration by a novel in vivo technique. *Blood*. 2005;106:3691-3698.

27. Krams R, Cheng C, Helderman F, Verheye S, van Damme LC, Mousavi Gourabi B, Tempel D, Segers D, de Feyter P, Pasterkamp G, De Klein D, de Crom R, van der Steen AF, Serruys PW. Shear stress is associated with markers of plaque vulnerability and mmp-9 activity. *EuroIntervention*. 2006;2:250-256.

28. Krams R, Verheye S, van Damme LC, Tempel D, Mousavi Gourabi B, Boersma E, Kockx MM, Knaapen MW, Strijder C, van Langenhove G, Pasterkamp G, van der Steen AF, Serruys PW. In vivo temperature heterogeneity is associated with plaque regions of increased mmp-9 activity. *Eur Heart J*. 2005;26:2200-2205.

29. Krams R, Wentzel JJ, Oomen JA, Vinke R, Schuurbiers JC, de Feyter PJ, Serruys PW, Slager CJ. Evaluation of endothelial shear stress and 3d geometry as factors determining the development of atherosclerosis and remodeling in human coronary arteries in vivo. Combining 3d reconstruction from angiography and ivus (angus) with computational fluid dynamics. *Arterioscler Thromb Vasc Biol*. 1997;17:2061-2065.

30. Bourantas CV, Papafaklis MI, Garcia-Garcia HM, Farooq V, Diletti R, Muramatsu T, Zhang Y, Kalatzis FG, Naka KK, Fotiadis DI, Onuma Y, Michalis LK, Serruys PW. Short- and long-term implications of a bioresorbable vascular scaffold implantation on the local endothelial shear stress patterns. *JACC Cardiovasc Interv*. 2014;7:100-101.

31. Bourantas CV, Papafaklis MI, Lakkas L, Sakellarios A, Onuma Y, Zhang YJ, Muramatsu T, Diletti R, Bizopoulos P, Kalatzis F, Naka KK, Fotiadis DI, Wang J, Garcia Garcia HM, Kimura T, Michalis LK, Serruys PW. Fusion of optical coherence tomographic and angiographic data for more accurate evaluation of the endothelial shear stress patterns and neointimal distribution after bioresorbable scaffold implantation: Comparison with intravascular ultrasound-derived reconstructions. *Int J Cardiovasc Imaging*. 2014;30:485-494.

32. Koskinas KC, Chatzizisis YS, Papafaklis MI, Coskun AU, Baker AB, Jarolim P, Antoniadis A, Edelman ER, Stone PH, Feldman CL. Synergistic effect of local endothelial shear stress and systemic hypercholesterolemia on coronary atherosclerotic plaque progression and composition in pigs. *Int J Cardiol*. 2013;169:394-401.

33. LaMack JA, Himburg HA, Zhang J, Friedman MH. Endothelial gene expression in regions of defined shear exposure in the porcine iliac arteries. *Ann Biomed Eng*. 2010;38:2252-2262.

34. Khan OF, Sefton MV. Perfusion and characterization of an endothelial cell-seeded modular tissue engineered construct formed in a microfluidic remodeling chamber. *Biomaterials*. 2010;31:8254-8261.

35. Kumar S, Sud N, Fonseca FV, Hou Y, Black SM. Shear stress stimulates nitric oxide signaling in pulmonary arterial endothelial cells via a reduction in catalase activity: Role of protein kinase c delta. *Am J Physiol Lung Cell Mol Physiol*. 2010;298:L105-116.

36. Urso C, Caimi G. [oxidative stress and endothelial dysfunction.]. *Minerva Med*. 2011;102:59-77.

37. Kuhlmann MT, Cuhlmann S, Hoppe I, Krams R, Evans PC, Strijkers GJ, Nicolay K, Hermann S, Schafers M. Implantation of a carotid cuff for triggering shear-stress induced atherosclerosis in mice. *J Vis Exp*. 2012;pii: 3308

38. Abela GS. Cholesterol crystals piercing the arterial plaque and intima trigger local and systemic inflammation. *J Clin Lipidol*. 2010;4:156-164.

39. Davies PF. Hemodynamic shear stress and the endothelium in cardiovascular pathophysiology. *Nat Clin Pract Cardiovasc Med.* 2009;6:16-26.

Figure Legends:

Figure 1. (A) Box and whisker plot of plaque burden computed as plaque (or intima) area divided by media area for each histological section and scaled by an assumed normal intima-

media areal ratio of 0.225 (linear ratio is 0.3). Plaque burden was ~3-fold higher downstream of the SMS compared to the SMS upstream and control artery segments (***p<0.001). Red dots indicate outliers. (B) Representative histological sections of advanced plaque types in the vessel segment downstream of the SMS. Advanced lesions were identified based on the presence of a necrotic core, inflammation (i.e., accumulation of macrophages), and presence of a fibrous cap. TCFA was defined when fibrous cap thickness was ≤65 μm (white arrow indicates TCFA cap in 10x picrosirius red image, which is further magnified to 40x in the entire bottom row of images). The white box in each 2x image indicates region of 10x image.

Figure 2. (A) Representative FD-OCT images of the maximum stenosis within the implanted SMS at 0 (baseline), 0+ (immediately post-SMS), 19, and 34 weeks showing increased severity of the stenosis due to intimal hyperplasia. (B) Maximum areal stenosis (%) averaged over all pigs, which increased from 0+ to 34 weeks (***p<0.001). (C) Mean inlet blood velocity (m/s) decreased in the instrumented artery over time (*p<0.02 compared to baseline), whereas the contralateral control artery did not significantly change. (D) Box and whisker plot of the relative change from baseline of 8 WSS metrics (see Supplemental Methods for list and definitions) in the instrumented downstream segment, computed as the difference of each metric from baseline over all pigs and all post-SMS implant time points and then scaled by the maximum median of all metrics (WSS). The parameters in which SMS implant caused the greatest positive change were LSI, HSI, and tSS. (E) Blood velocity and streamlines from CFD in the instrumented and contralateral control arteries of one representative pig. The instrumented vessel exhibits high flow on the outer and low and multidirectional flow on the inner curvature, whereas the control artery maintains a normal and nearly homogeneous flow profile. At select axial locations in each

vessel, cross-sections are provided to show the distribution of velocity. In the bar plots (B and C), data are expressed as mean±SD.

Figure 3. LSI, HSI, and tSS grouped by plaque type (advanced – TCFA, FCA, and PIT; early – IT and XA, and normal wall) within each of the vessel segments at immediately post-SMS implantation (time=0+) and scaled by the maximum value of the 3 metrics (LSI). (A) Of all WSS metrics, LSI had the highest relative magnitude within advanced lesions in the instrumented downstream segment, which was statistically higher than LSI within advanced lesions of other vessel segments (**p<0.002) and other plaque groups in the downstream segment (**p<0.002). (B) HSI was nearly exclusively present in the instrumented downstream segment. Interestingly, maximal values within this segment were lowest in advanced lesions compared to early lesions (**p<0.002) and normal wall (**p<0.002). (C) tSS was similar to LSI with highest values in regions of advanced lesions within the instrumented downstream segment that were statistically different from those in other segments (**p<0.002) and different from early lesions (**p<0.002) and normal wall (**p<0.002) in the downstream segment. *Indicates statistically higher values of the given WSS metric within the plaque group designated by the bar over which it is placed versus the same plaque group in other vessel segments (control – Δ, instrumented upstream – Θ, and instrumented downstream – Ξ) and different plaque groups within the same segment (advanced – χ, early – ψ, and normal – ω). Data are expressed as geometric mean plus upper limit of 95%CI.

Figure 4. (Top row) Representative 3-D reconstruction of LSI within one pig over time (location of SMS indicated by grey lines). (Remaining rows) Panels are obtained by computationally

isolating the downstream segment (indicated by the black box in the 3-D representation), opening the vessel and laying it flat ("en-face" with the endothelium facing up) to demonstrate the patterns of LSI, tSS, and plaque type. LSI and tSS are scaled from 0 (null value, indicated by blue) to 1 (maximum value, indicated by red). Plaque type is displayed as a function of plaque burden, ranging from normal wall given by the flesh-color to the maximum plaque burden given by the highest color intensity of each plaque type (TCFA – red, FCA – green, PIT – blue, XA – violet, and IT – yellow). The histological data are obtained at the end time point (34 weeks) and then co-registered to the vessel reconstructions at each time point (see Supplemental Methods).

Figure 5. LSI, HSI, and tSS within each plaque type of the instrumented downstream segment, averaged over all sections containing that plaque type and all pigs at each time point. These shear metric values are scaled by the maximum over all shear metrics (LSI at 19 weeks) to facilitate comparisons. (A) Over all post-SMS implant times as a whole, LSI had a higher presence in regions of TCFA compared to FCA ($p<0.005$) and PIT ($p=0.25$), though the latter was not significant, and all advanced lesions exhibited a higher LSI compared to early lesions and normal vessel ($p<0.005$, except FCA versus XA where $p=0.90$). (B) HSI in the advanced lesions was generally lower than other plaque groups, except regions of FCA at 18 weeks ($p<0.005$) suggesting that this stimulus may have promoted the stable plaque phenotype. (C) tSS initially exhibited a statistically higher presence in regions of advanced plaques compared to early lesions and normal vessel ($p<0.005$) at immediately post-SMS implant, but it was not consistent over time. *Indicates statistically higher values of the given WSS metric within the advanced plaque type designated by the bar over which it is placed versus other plaque types (TCFA – α, FCA – β, PIT – γ, XA – δ, IT – ε, and NOR – ζ). Data are expressed as geometric mean plus upper limit of 95%CI.

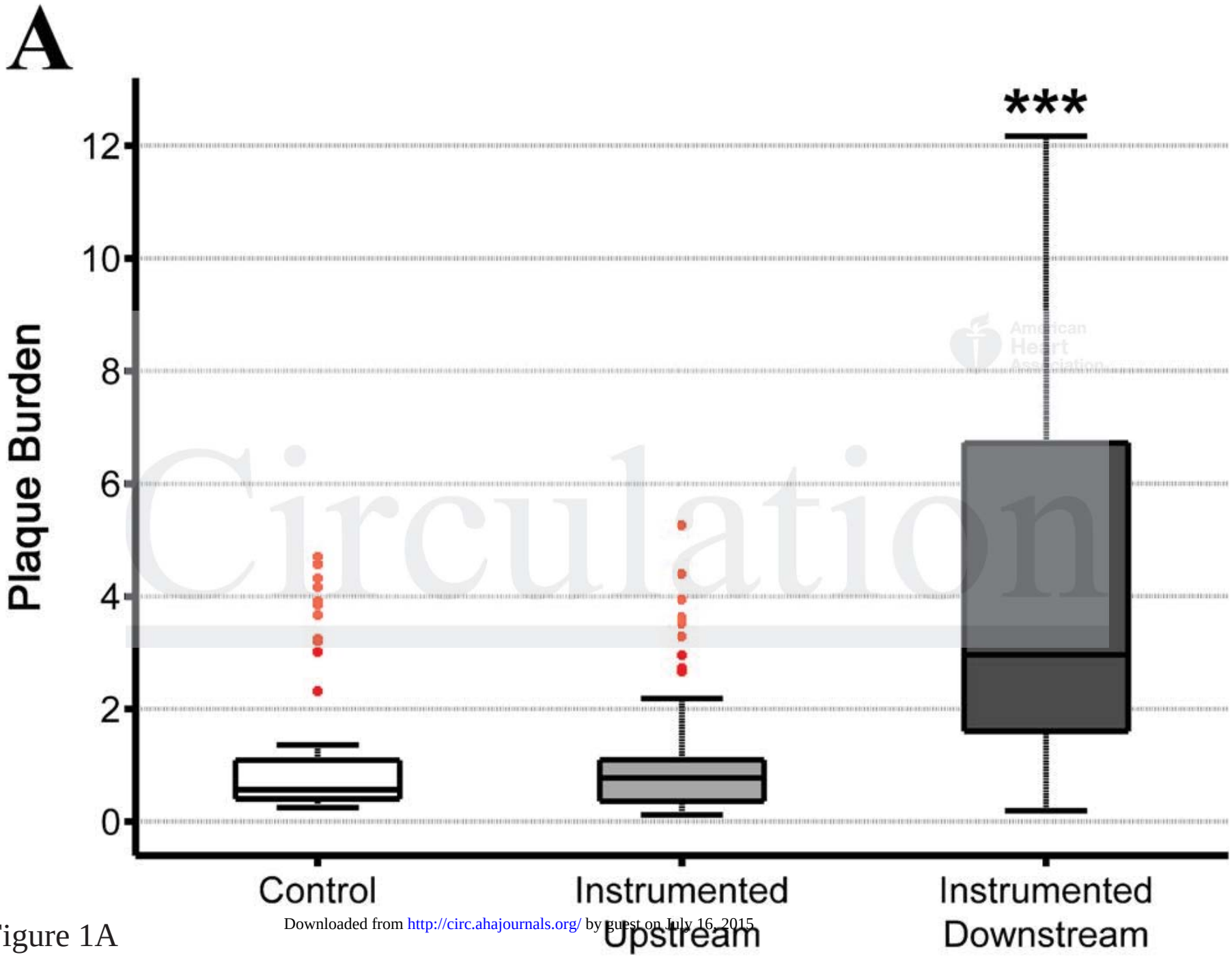

Figure 1A

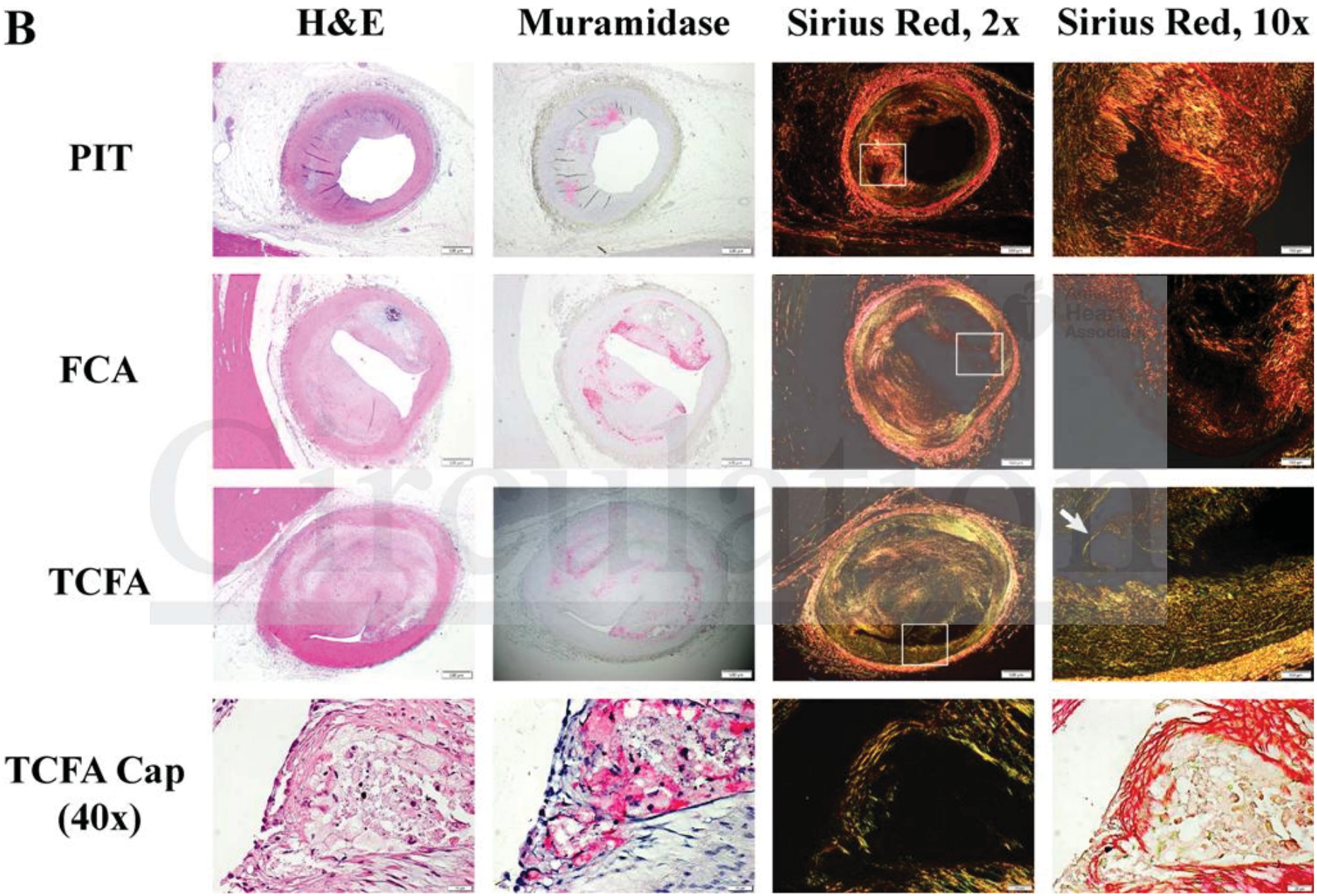

Figure 1B

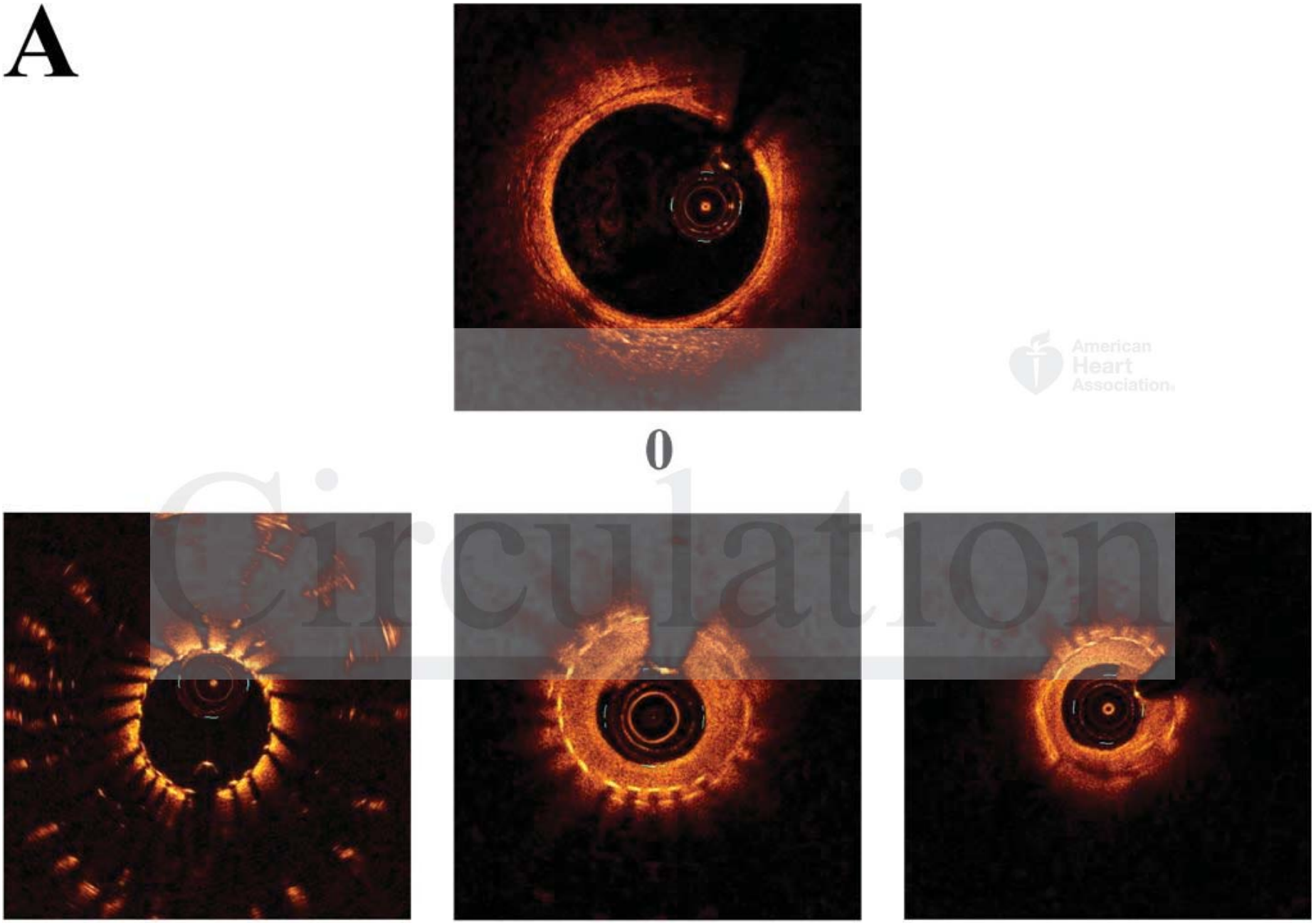

Figure 2A

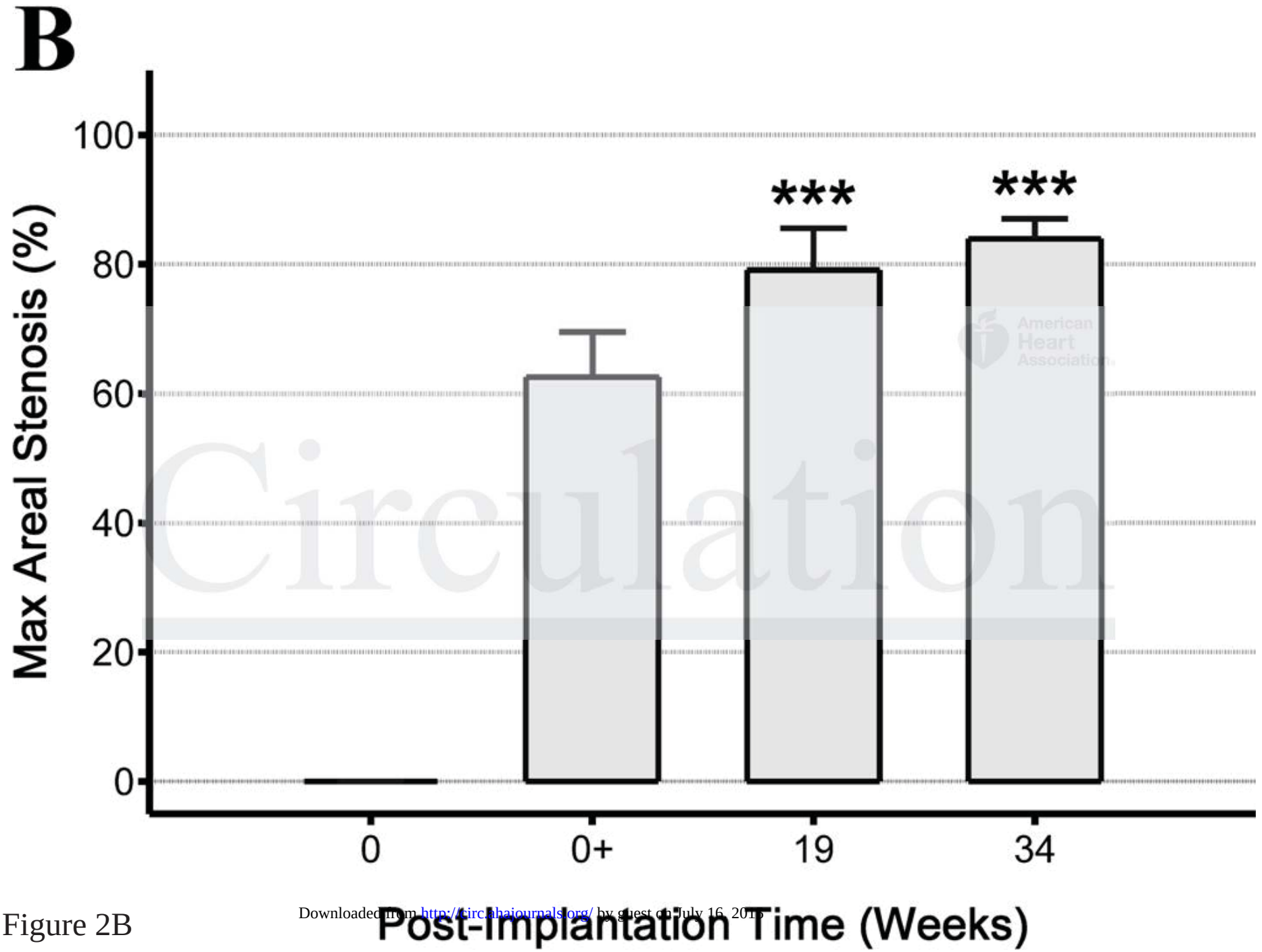

Figure 2B

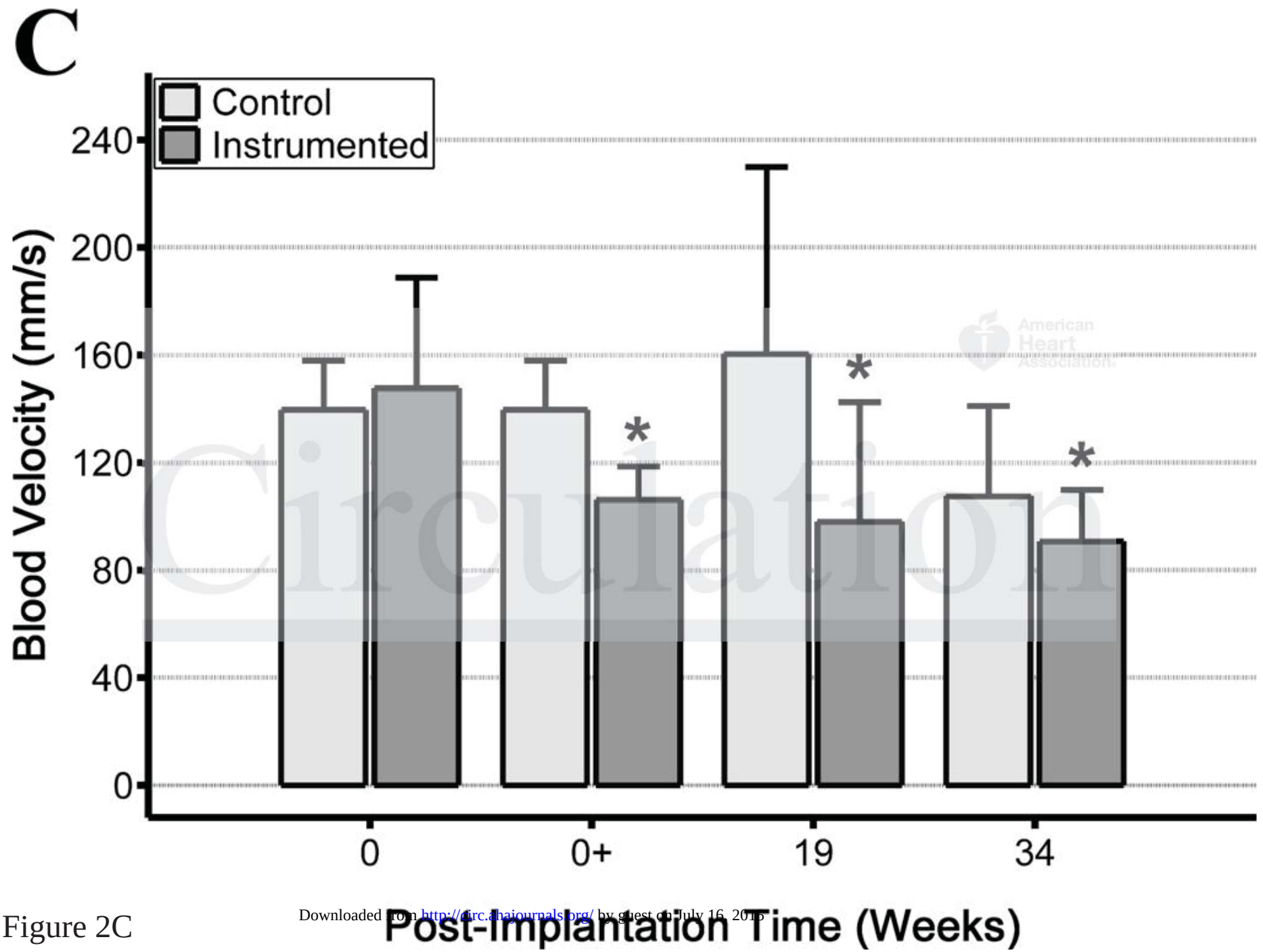

Figure 2C

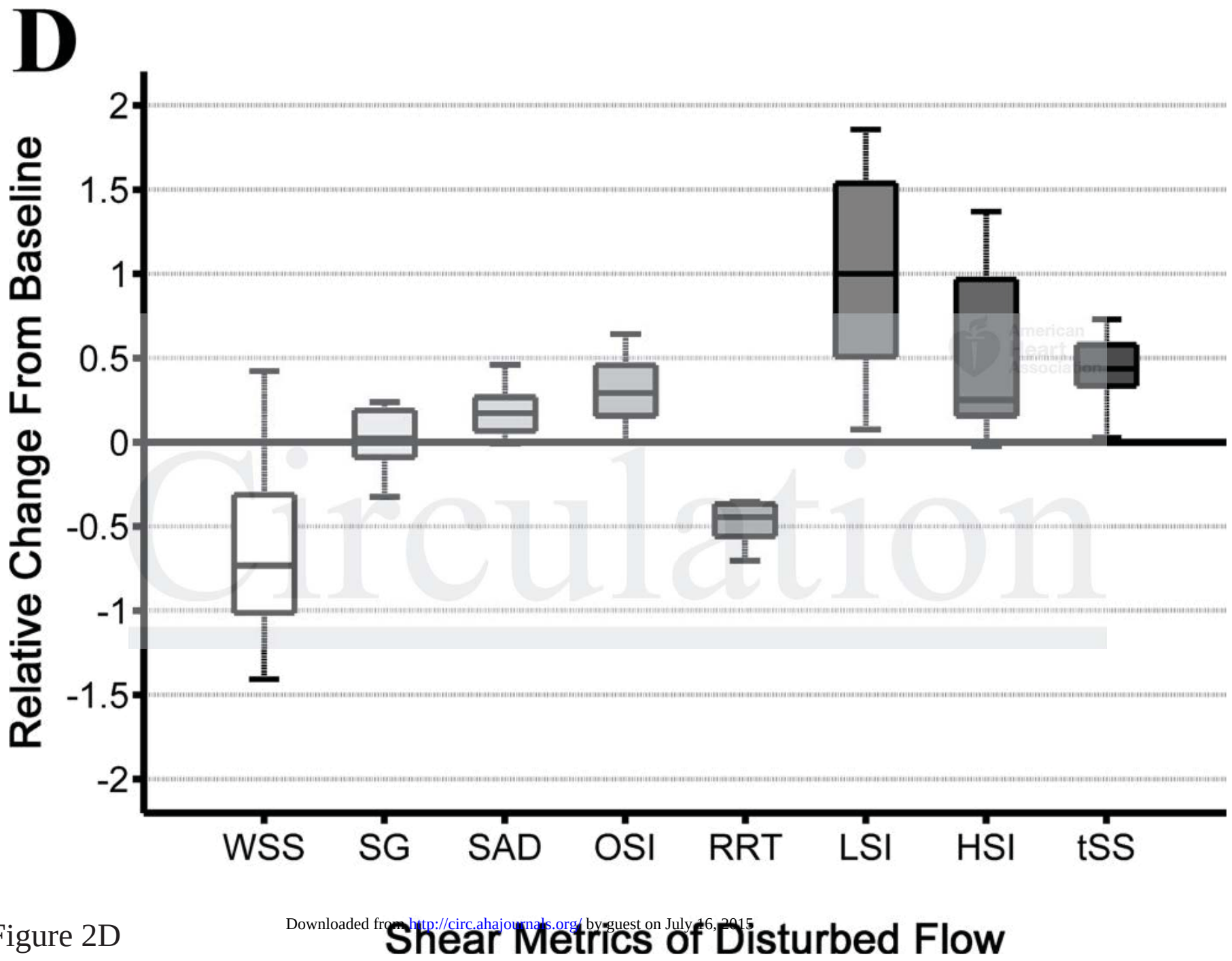

Figure 2D

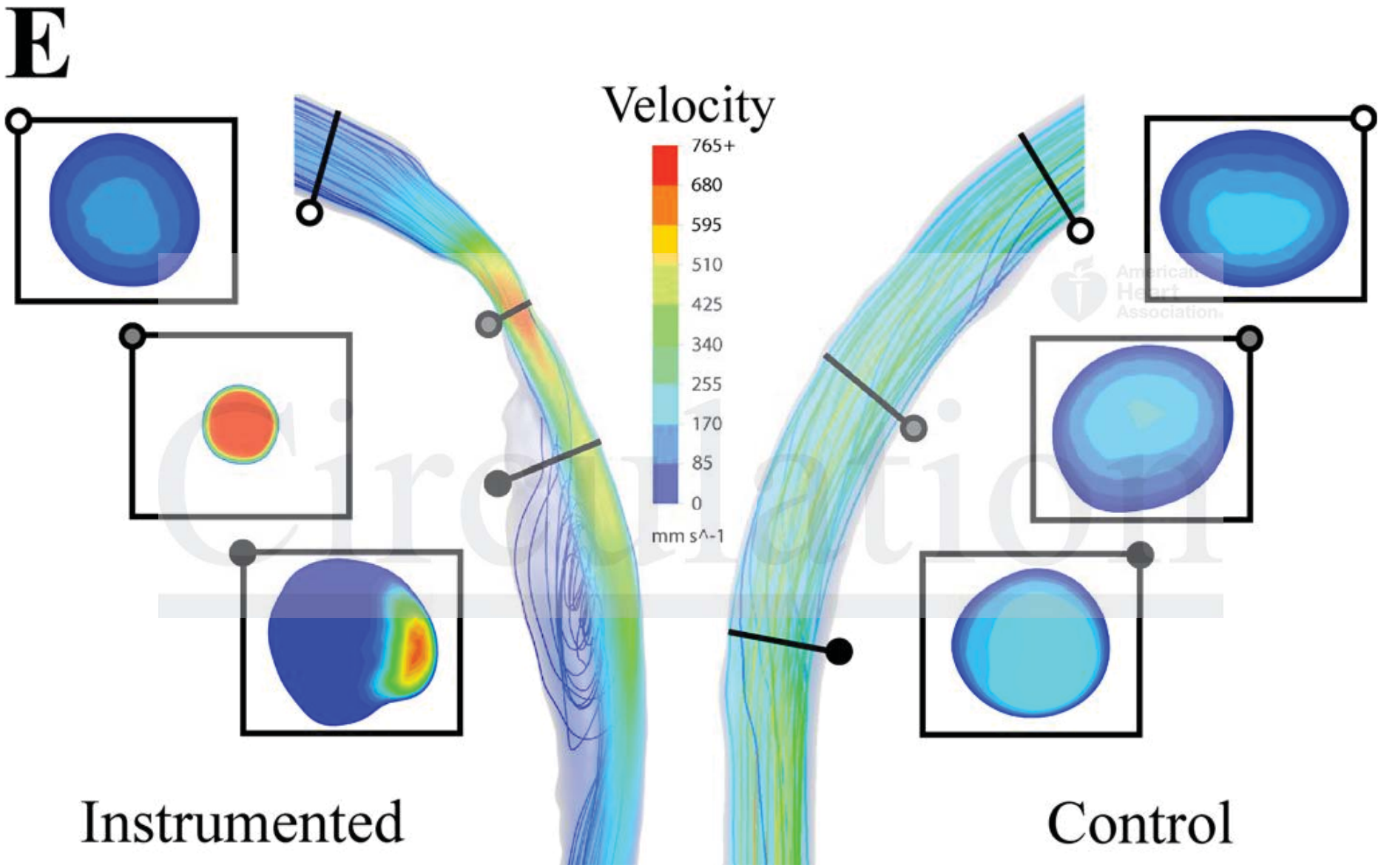

Figure 2E

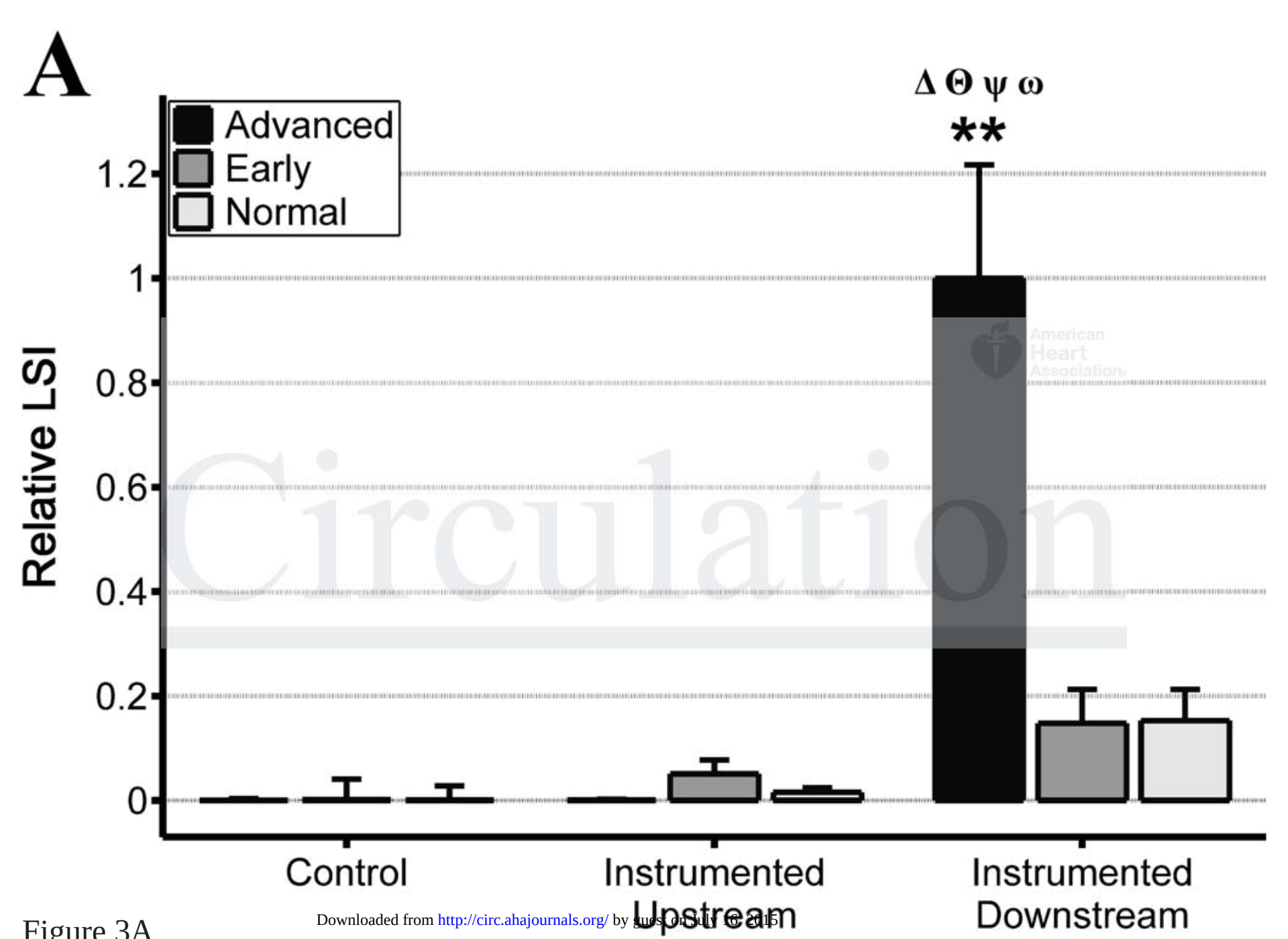

Figure 3A

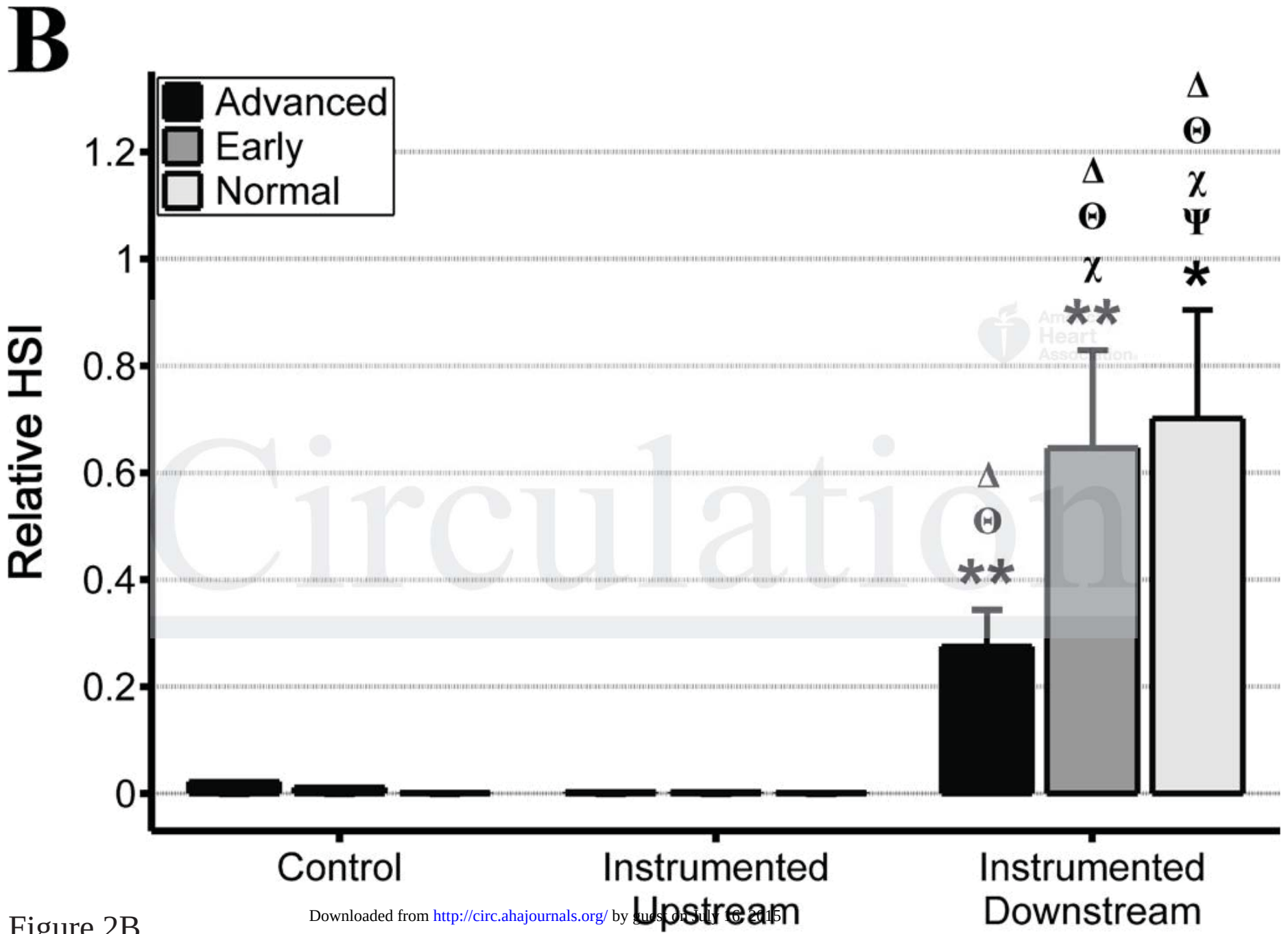

Figure 2B

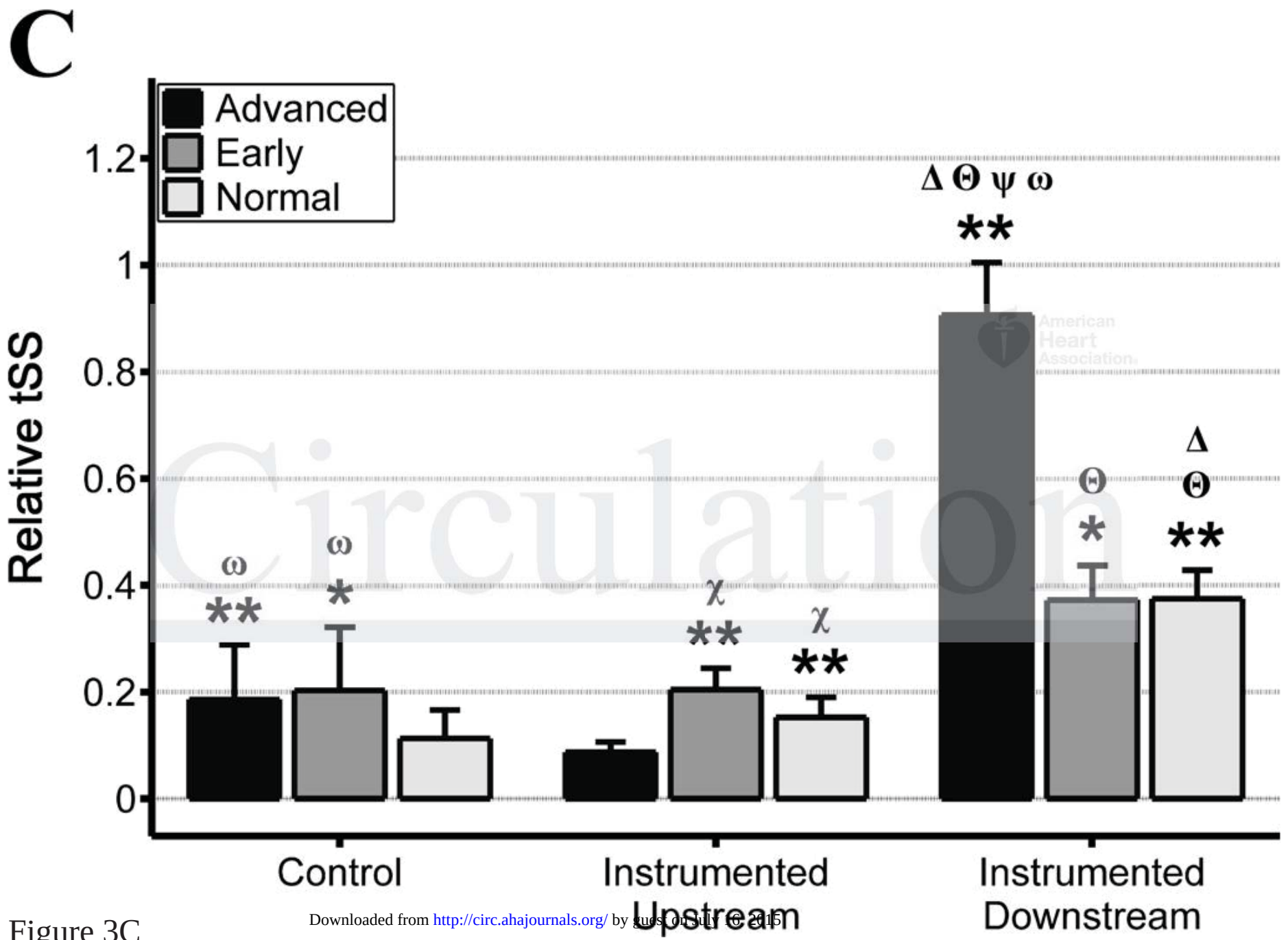

Figure 3C

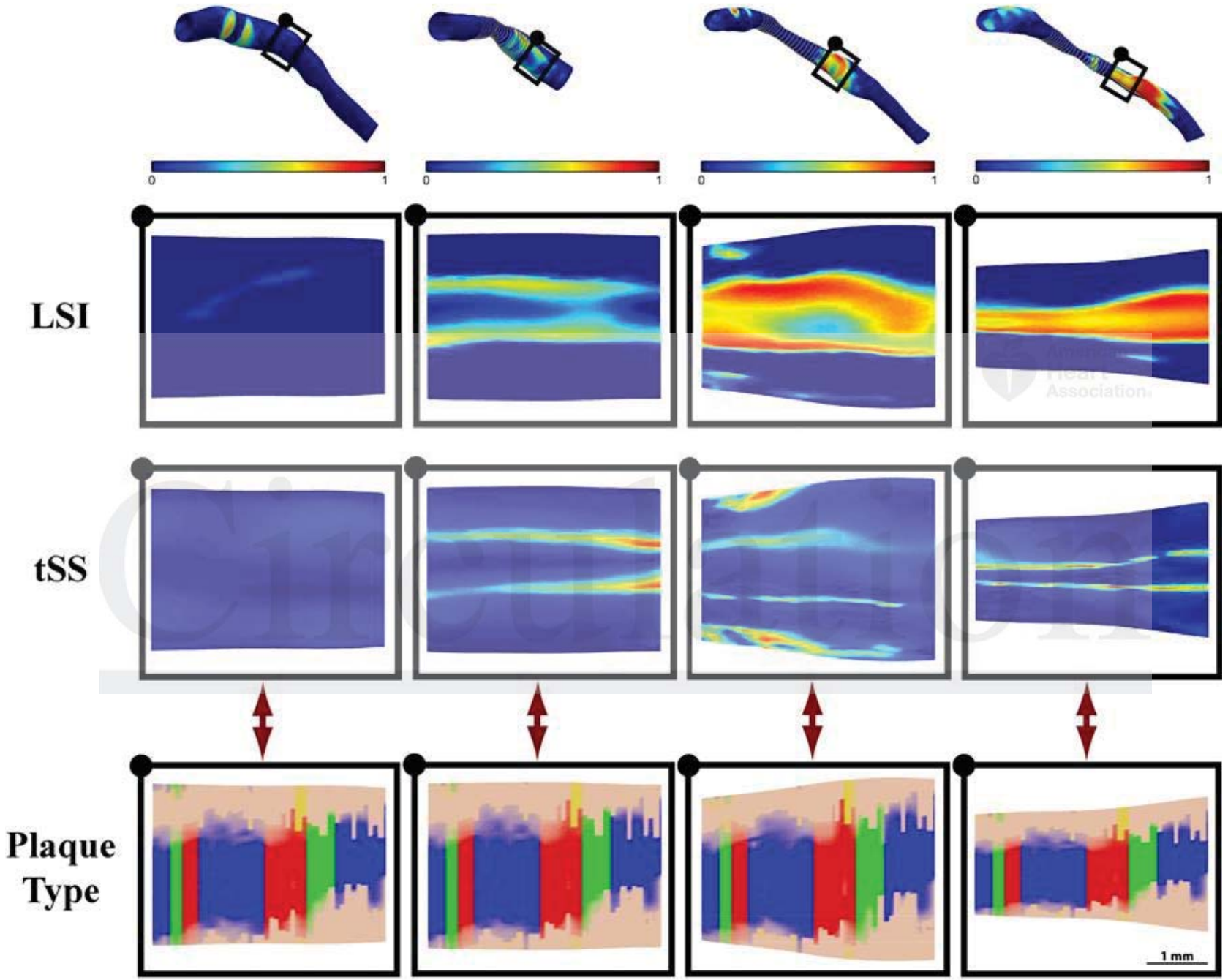

Figure 4

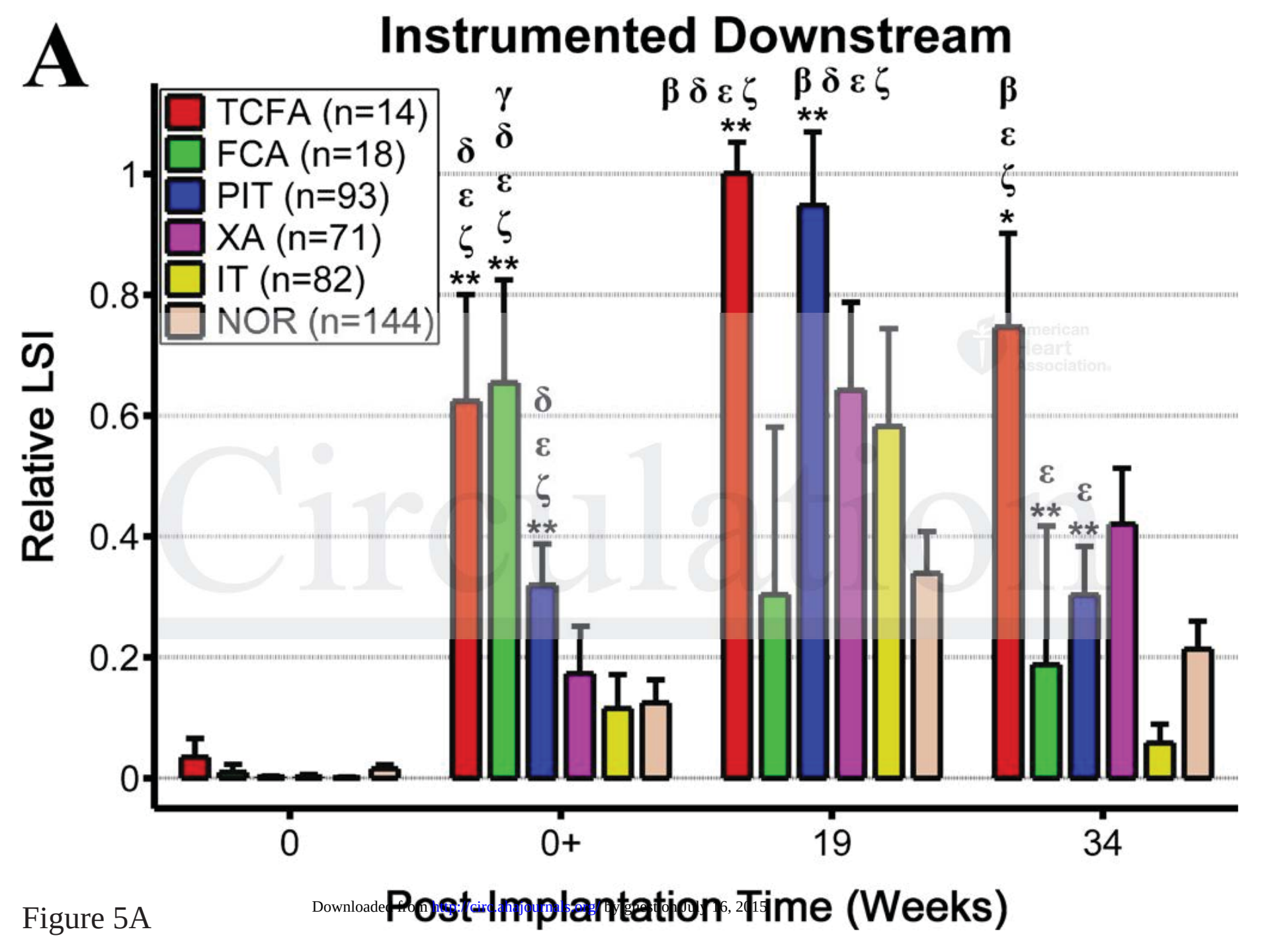

Figure 5A

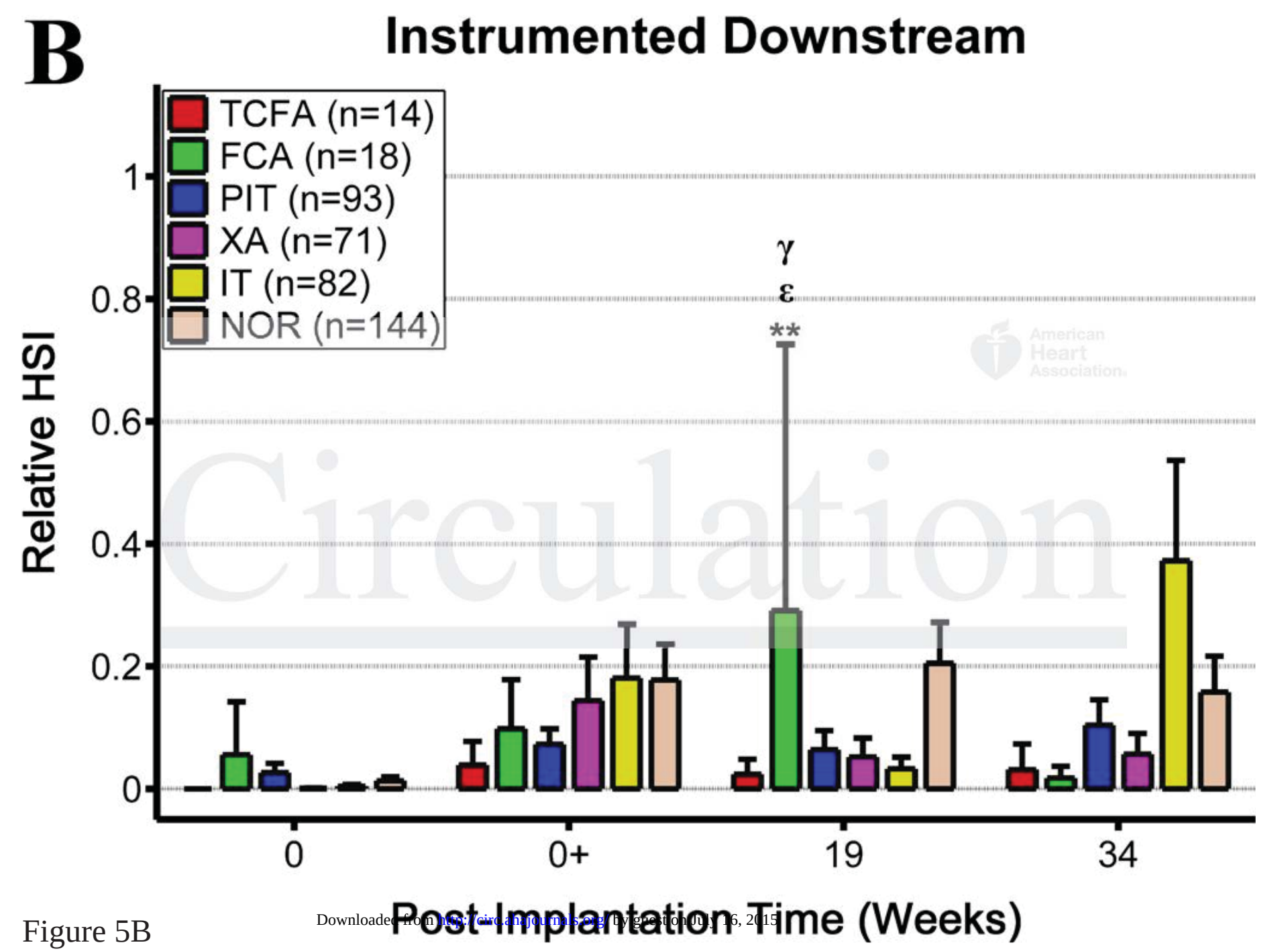

Figure 5B

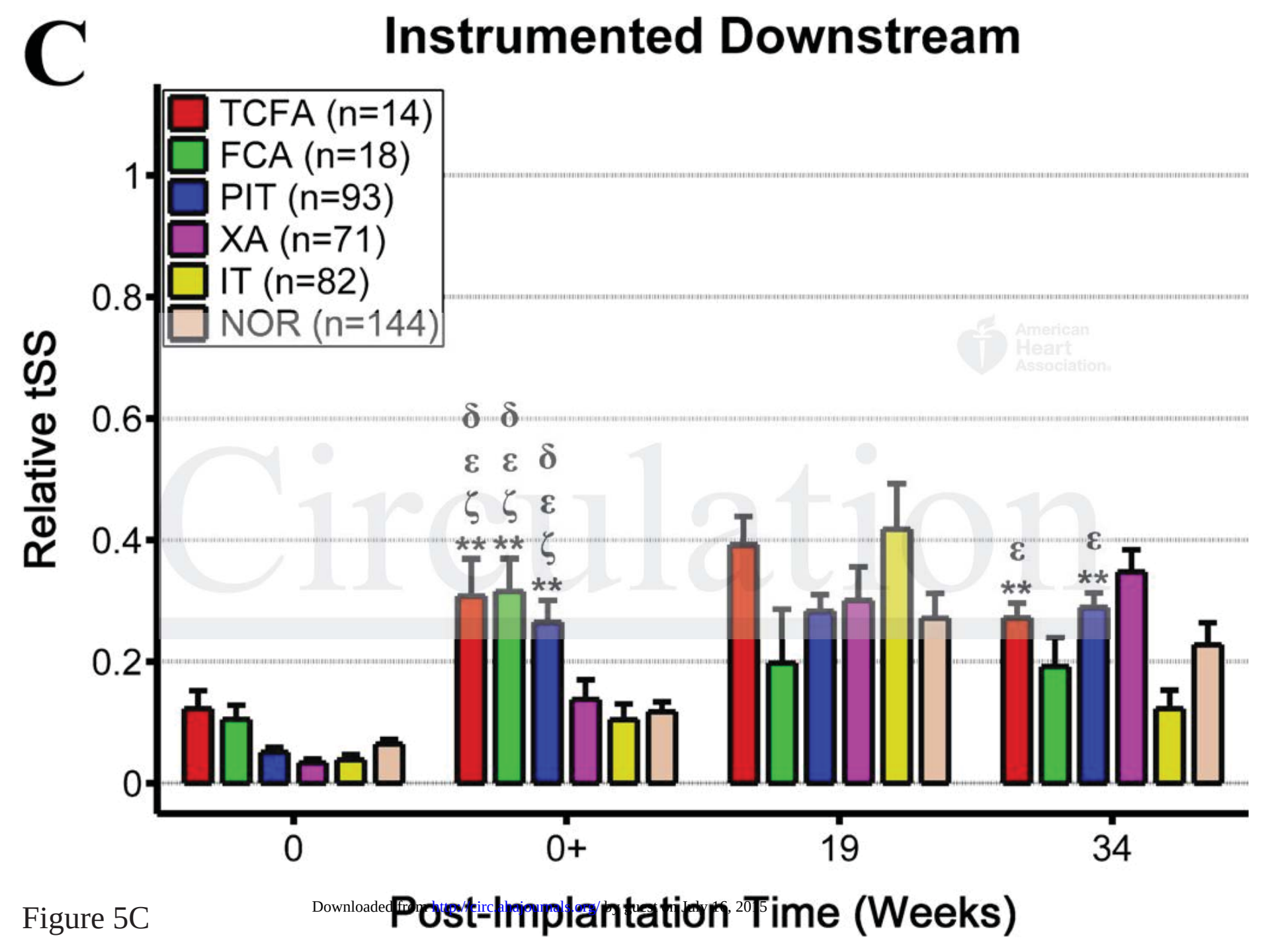

Figure 5C

SUPPLEMENTAL MATERIAL

Supplemental Methods

Animals

All animal experiments were performed in accordance with the ethical and welfare regulations of the University of Aarhus and approved by the Danish Animal Experiments Inspectorate. The study protocol is shown in Supplemental Figure 1. Six female *D3749* PCSK9 transgenic minipigs on a Yucatan background were fed a cholate free high fat high cholesterol (HFHC) diet consisting of 20% lard and 2% cholesterol (Sigma-Aldrich, UK) added to a standard pig diet of 68.0% barley, 15.0% oat, 9.6% soy bean meal, 2.0% animal fat 3.0% molasses, and 2.4% minerals and vitamins. Each pig received 700-900g HFHC diet divided into two portions daily for 1-4 months prior to instrumentation[1]. During the study, the weight of the animals increased from 48 ± 2 kg (mean +/- SD) at baseline to 75 ± 2 kg at the end of the protocol (34 weeks).

The day before each catheterization procedure, pigs were fasted overnight with access to drinking water *ad libitum*. On the day of each procedure, pigs were pre-medicated with a weight-adjusted mixture of 0.5 mg/kg of midazolam (Accord Healthcare, Gothenburg, Sweden) and 4 mg/kg of azaperone (Janssen Animal Health, Beerse, Belgium) before anesthesia induction using 0.5 mg/kg of intravenous etomidate (Hypnomidate, Janssen-Cilag, UK). Following endotracheal intubation, the pigs were mechanically ventilated with 60% oxygen in pressure regulated volume-controlled mode (S/5 Avance, Datex-Ohmeda, GE Healthcare, UK). Anesthesia was maintained with Sevoflurane (Abbvie A/S, Denmark), to a mean alveolar concentration (MAC) of 1.2 to 1.4%, together with continuous intravenous infusion of fentanyl 0.02 mg/kg/hr (Hameln Pharmaceuticals, Germany). During the procedure, continuous monitoring of electrocardiogram, oxygen saturations, end-tidal CO_2 and arterial blood pressure was performed. At the time of all interventional procedures, the

pigs received 1g of intravenous ampicillin (PharmaCoDane, Herlev, Denmark) before and after the catheterization procedures.

Shear-modifying stent implantation and follow-up cardiac catheterization procedures

One week prior to implant of a stenotic shear modifying stent (SMS)[2], all pigs received 300 mg aspirin (Takeda Pharma, Roskilde, Denmark) daily. 300 mg of clopidogrel (Actavis Group, Hafnarfjördur, Iceland) was administered 24 hours beforehand. To minimize peri-procedural arrhythmia, the animals were pre-treated with 25 mg atenolol (Takeda Pharma) once daily and 200 mg amiodarone (Sandoz, Copenhagen, Denmark) twice daily for one week pre- and post-procedure. After SMS implantation, all pigs received 75 mg of aspirin and 75 mg of clopidogrel once daily for the remainder of the study.

An 8F arterial sheath (Arrow International, Reading, PA, USA) was placed percutaneously under ultrasound guidance. Unfractionated heparin 5000u (LEO Pharma, Ballerup, Denmark) was administered intravenously and supplemented with a further 1000u each hour. The left coronary artery was engaged with an 8F Hockey Stick I guiding catheter. All angiographic acquisitions were performed with ventilation briefly paused during image acquisition to minimise respiratory motion artefacts and after administration of intracoronary isosorbide dinitrate (0.3-1.0 mg). Coronary angiograms were acquired in orthogonal views during injection of iodinated contrast (iohexol 140mgI/mL, GE healthcare, Oslo, Norway) using a clinical grade digital fluoroscopy suite (Allura Xper FD10, Philips, Eindhoven, The Netherlands). Coronary flow velocity was measured in the left anterior descending (LAD) and left circumflex (LCx) coronary arteries using a ComboWire (Volcano Corporation, San Diego, CA, USA). The ComboWire was advanced to the tip of the guide catheter, where aortic pressure and ComboWire pressures were equalized and then advanced into a proximal vessel segment at least 5 mm away from any major angiographic side branch (>2 mm

diameter) to measure the inlet velocity over 10 to 20 stable cardiac cycles. Intracoronary frequency domain optical coherence tomography (FD-OCT) was performed in both the LAD and LCx using the Illumien system and Dragonfly imaging catheters (St Jude, St. Paul, MN, USA). Prior to each pullback, the FD-OCT catheter was imaged in orthogonal views during injection of iodinated contrast to enable 3-D reconstruction of the catheter path within the artery. FD-OCT pullbacks at a speed of 20 mm/s were performed during pump injection of iohexol (4-8 mL/s). After completion of baseline measurements, a SMS was implanted in the LAD (N=1) and LCx (N=5). Coronary angiography, coronary flow velocity and FD-OCT measurements were repeated in the stented vessel. The non-stented artery served as a control.

Follow-up cardiac catheterization procedures and acquisition of coronary angiograms, coronary flow velocity and FD-OCT data in both the stented and control arteries were performed as above at 19 and 34 weeks after initial stent implantation.

Tissue preparation and histology

After the final catheterization procedure, a median sternotomy was performed under general anaesthesia and the heart exposed. Unfractionated heparin (10,000u) was injected intravenously followed by injection of 50 mL saturated potassium chloride solution (KPBS) into the ascending aorta under direct vision. The heart was excised and the coronary arteries flushed with KPBS. Next, the coronary arteries were perfusion-fixed at 100 mmHg for 1 hour, followed by immersion fixation for 24 hours in 4% formaldehyde diluted in PBS (VWR, Prolabo, Belgium), after which the heart was stored in PBS at 5^{o}C until further processing.

Before excision, the surface of each artery was marked with indelible Tissue Marking Dye (Triangle Biomedical Sciences, Durham, NC, USA) that was visible on histological sections, which, together with the attached myocardium, served as circumferential fiducial

markers for subsequent co-registration of each histology section to the corresponding location on the 3-D artery reconstructed from FD-OCT. 5 mm tissue blocks containing the coronary artery and underlying myocardium were cut immediately distal and proximal to the SMS edges. In each uninstrumented control artery, a 5 mm tissue block was excised at an axial position that was at a comparable distance from the left main bifurcation as the proximal edge of the stent in the instrumented vessel. At each step in the histology processing, the coronary arteries were photographed with an adjacent reference scale to enable estimation of change in arterial length resulting from each individual processing step.

Sections from each 5 mm tissue block were collected at 3 μm-thick intervals over a distance of 2.5 mm in the blocks adjacent to the stent and 1 mm in the control, and stained with haematoxylin and eosin (H&E), picrosirius red (collagen), and muramidase (pan macrophage marker). For the latter, we used a modified version of the protocol described by Falk et al[3]. Briefly, proteolytic antigen retrieval (Dako Cytomation S3007) was performed followed by Protein Block (X0909, Dako , USA), both for 10 minutes. The primary antibody (Dako, muramidase polyclonal rabbit anti-human antibody, diluted 1:500) was applied for 2 hours at room temperature. Subsequently, a biotinylated secondary antibody (Dako Cytomation Multilink, diluted 1:100) and streptavidin-alkaline phosphatase (Vector Laboratories SA-5100, diluted 1:500) was applied for 30 min each. Staining was detected with Permanent Red (Dako Cytomation), after which the slides were dehydrated, cleared, and cover-slipped. Digitized images of the histology sections were acquired using an Olympus BX50 light microscope with a Colorview 2 camera.

3-D artery reconstruction and computational fluid dynamics

The 3-D geometries of the instrumented and control arteries were obtained by placing lumen contours segmented from FD-OCT frames along the path of the catheter during

pullback. The catheter path was defined by reconstructing the 3-D shape of the Dragonfly catheter from orthogonal angiographic frames using the CASS 5.11 software (Pie Medical, Netherlands) and then obtaining the centreline of this reconstruction using the Vascular Modelling Toolkit (VMTK, Orbix, UK). Contours of the vessel lumen and plaque distributions were segmented from each frame of the FD-OCT pullbacks using a commercial imaging workstation (St Jude Medical) and echoPlaque 4.0 (Indec Medical Systems, Santa Clara, CA, USA). Only clear image frames with visible lumen and vessel wall for $>270^{o}$ continuous arc were analyzed. Whenever a side branch was present in an OCT image, the lumen was segmented as if no side branch were present. To obtain the final *in vivo* 3-D geometry of the artery from FD-OCT, the catheter path and frame contours (lumen and plaque) were loaded into custom software developed in Matlab (Mathworks, Natick, MA, USA) that performed three primary functions. First, the location of each frame was determined by the speed of the catheter pullback. Second, to place the contours normal to the reconstructed catheter centerline and to account for catheter torsion, a discrete approximation to the Frenet–Serret formulae[4] was employed to identify the relative orientations of each contour. Finally, to determine the absolute orientation of each contour, a single rotation angle around the catheter centerline was calculated for all contours by using the out-of-centre vector approach described by Wahle et al.[4] For this approach, the FD-OCT reconstruction is compared to an angiography reconstruction of the vessel that was obtained using the CASS 5.11 software (Pie Medical, Maastricht, Netherlands). The points of all contours along the catheter path represent the *in vivo* lumen surface, which was then smoothed in VMTK. This approach enables 3-D reconstruction of the artery in its *in vivo* conformation from the FD-OCT data. We validated the approach with a detailed error propagation analysis (see below), vessel phantoms, and a pilot pig study[5].

The 3-D reconstruction of the arterial lumen from FD-OCT data was used for computational fluid dynamics (CFD) simulations to compute wall shear stress metrics of disturbed flow and perform 3-D histology (Supplemental Figure 1). The lumen surface was meshed using a combination of ICEM CFD (Ansys, Pittsburgh, PA, USA) and Gambit version 2.4.6 (Ansys). The mesh was then imported into the commercial package Fluent version 6.3 (Ansys) to numerically solve the Navier-Stokes equations of motion for a fluid. In addition to defining the lumen geometry, properties of the fluid and boundary conditions were also prescribed within the model. Blood was assumed to be an incompressible Newtonian fluid with a viscosity of 3.5 mPas[6] and density of 1050 kg/m^3.[7] Simulations imposed a pulsatile flow of the blood at the inlet of the vessel by assigning a plug flow profile equal to the peak velocity measured at each point in the cardiac cycle.[8] The corresponding velocity wave form represented the average wave form over all cardiac cycles acquired with the ComboWire. The inlet was also extended to allow the flow to become fully developed before entering into the actual lumen reconstruction. The outlet of the vessel had a prescribed pressure of 0 mmHg. The lumen surface was assumed to be stationary with a no-slip boundary condition.

The primary output of the CFD simulations was a wall shear stress vector at each point on the lumen surface and at each point in the cardiac cycle (broken into 20 time steps for the simulation), which were then imported into a custom Matlab program to quantify metrics of local hemodynamics (primarily disturbed flow), including: time-averaged wall shear stress (WSS)[9], oscillatory shear index (OSI)[10, 11], relative residence time (RRT)[12], wall shear stress gradient (SG)[9], wall shear stress angle deviation (SAD)[13] and the recently developed transverse wall shear stress (tSS), which considers the multi-directionality of the flow field[14, 15] (Supplemental Table 1). In addition to these established metrics, we developed two new WSS metrics, the low shear index (LSI) and the high shear index (HSI).

Development of these metrics was motivated by having data on the shear stress profile of the SMS-implanted artery prior to its placement at baseline when the artery has physiological flow and is non-atherosclerotic, as well as after SMS implantation, which perturbs flow and causes atherogenesis. We reasoned that metrics quantifying regional differences in WSS at each post-instrumented time point compared with baseline, may identify the types of flow disturbance that are most atherogenic. Although this approach could be used to examine longitudinal changes in multiple descriptors of local flow conditions, we initially focused on changes in WSS magnitude. LSI quantifies reduction in WSS, with its value increasing as WSS reduces. By contrast, HSI is a measure of an increase in WSS, with its value increasing as WSS increases. The thresholds for LSI and HSI were determined by normalizing, via log-transformation, the baseline WSS values of the instrumented vessel before SMS placement, after which the bottom and top 10^{th} percent of the distribution (equal to 1.28*standard deviation) were used for each metric, respectively. Exponential transformation of these two values was used to obtain the absolute threshold values of WSS for discriminating low and high WSS. Values of WSS at each point on the 3-D reconstructed artery after SMS implantation were compared to the LSI and HSI threshold values from baseline at each post-stent time point to characterize the degree of low or high WSS on a continuous scale (for example, WSS at points on the vessel lumen below the LSI threshold would have positive LSI values, whereas those above the LSI threshold would have LSI values equal to 0). This definition of low and high WSS allows for a window of normal shear, thus the absence of one metric does not imply the presence of the other.

Analysis to determine shear stress within each plaque type

To quantify spatial overlaps between WSS metrics and histopathological features of atherosclerosis, we co-registered histology information to the reconstructed *in vivo* lumen

from FD-OCT through a multi-step process termed 3-D histology, which we first described in previous work in the rabbit aorta[16]. First, 3 μm-thick histology sections were serially collected over the first 2.5 mm of the block (equivalent to ~4.5 mm *in vivo*). In control tissue blocks, only 1.0 mm was assessed (equivalent to ~1.7 mm *in vivo*). Sections were sequentially microtomed and organized onto 10 alternating slides, each with 2 adjacent sections per slide, resulting in an interval between slides of 6 μm to allow evaluation of up to 10 stains over the length of the segment. This method provided an interval of 60 μm between sections for a given stain. Plaque type and morphology were classified at 60 μm intervals according to the Virmani classification by expert histopathologists (authors CBP and EF) who were blinded to the CFD and FD-OCT data[17]. Plaques were categorized as thin-cap fibroatheroma (TCFA), fibrous cap atheroma (FCA), pathological intimal thickening (PIT), xanthoma (XA), intimal thickening (IT), or normal vessel wall (NOR) and a color coding system (red for TCFA, green for FCA, blue for PIT, pink for XA, yellow for IT, and black for NOR) was used to delineate plaque type on a local (i.e., point-to-point) basis within each H&E-stained section (Supplemental Figure 2) using Microsoft Paint (Microsoft, Redmond, WA, USA). The analysis was either performed on individual plaque types or plaque types grouped as advanced (TCFA, FCA, and PIT), early (defined as XA and IT), or non-diseased/normal (NOR). Regarding the determination of progressive lesions, PIT was classified based on the presence of foam cells, extracellular lipid, and/or calcium depositions. FCA was classified based on the presence of a necrotic core containing necrotic cells and the absence of collagen, determined from the H&E and picrosirius red stains. Fibrous cap thickness was measured on the picrosirius red stain using Image J version 1.46 (NIH, USA) and fibroatheromas with a cap thickness less than or equal to 65 μm were designated as TCFA[17].

On the digitized histology sections, the lumen, internal elastic lamina, and external elastic lamina contours for the H&E stain were segmented (Clemex Technologies, Longueuil, QC, Canada). A custom Matlab program was developed, based on previous work in our group[16, 18, 19], to discretize contours with the same number of equidistantly spaced, user-defined nodes circumferentially (100) as were contained in the reconstructed vessel (composed of FD-OCT frames). The intima to media ratio was computed at each circumferential point of each histology section to quantify plaque burden. Contours were circumferentially aligned using the myocardium as a reference and co-registered with the 3-D vessel reconstructed from FD-OCT images at the point of maximum inner curvature, as the artery courses over the surface of the curved myocardium *in vivo*. Thus, this approach corrects for rotational artefacts and shrinkage about the radial and circumferential directions. Co-registration about the axial direction of the vessel (i.e., its long-axis) was based on the identification of bifurcations in both histology sections and FD-OCT frames and, in the instrumented vessel, the stent, which, together with images of vessel segments taken at each stage of tissue processing for histology, allowed computation of a shrinkage factor. The mean (±SD) shrinkage factor from the loaded, *in vivo* vessel to post-processing for histology was 41±6% and 45±4% in the control and instrumented vessel segments, respectively, which was not statistically different (p=0.39). To ensure the same vessel region was always identical over time, the length of each in vivo vessel segment at each time was scaled by the ratio of the original length at the current time compared to the final time point (34 weeks), based on identified anatomical landmarks (i.e., the stent and bifurcations). Using this overall approach, the range of FD-OCT frames acquired for a particular vessel segment can be matched to the serially-collected histology sections, whose interval is constant over that segment. A linear interpolation function in Matlab was used to interpolate plaque burden measures at each point of each histology section over the reconstructed vessel segment corresponding to the

identified FD-OCT frames. A similar interpolation approach was used for plaque type, wherein in-between values of each RGB color vector (indicating plaque type) were rounded to the nearest plaque type by computing a "distance" between each possible color vector and using the minimum as the nearest color.

Following this co-registration process, every node in both the reconstructed *in vivo* vessel segment and histological sections contained several metrics: coordinates, WSS metrics of disturbed flow, plaque type, and plaque burden. The magnitude of each WSS metric within each plaque type was then determined on a local scale. To avoid artificially inflating statistical power, each histological section was treated as a separate, repeated measurement within each pig. Thus, the mean WSS metric for each plaque type was determined on a per histological section basis, which corresponds to 60 μm axial increments within the histological block and ~105 μm increments *in vivo*. Because the axial resolution of FD-OCT is 200 μm, we used a linear interpolation function in Matlab to re-discretize the reconstructed *in vivo* vessel segment into a grid with a higher resolution of nodal spacing axially that enabled matches with the histological sections. To facilitate comparisons between WSS metrics, all metrics were scaled to create a continuous range of severity from 0 (null value) to 1 (the maximum severity of the type of flow disturbance detected by that metric). WSS, SG, and RRT were scaled by the maximum value within each vessel, OSI, LSI, and HSI were scaled by the theoretical maximum value (0.5, 100, and 100, respectively), SAD was scaled by the number π (assuming that an angle deviation of 180^{o} is the maximum disturbance), and tSS was scaled by the WSS at each respective point in the vessel (the theoretical maximum of the metric). Because tSS is scaled by a changing factor, the resultant spatial patterns may differ from the original metric. Although scaling can be subjective, it is necessary to determine the functionality of each WSS metric and it enables construction of a hierarchy of the relative contributions of the type of flow disturbance described by each metric, and their

combinations, to the development of different atherosclerotic plaque types. Next, a threshold of 0.1 was also imposed to de-noise the data, based on the error in computing WSS of 10% within our system (see *Error Analysis* section). Finally, the primary readout was the mean of each WSS metric within each of the plaque types identified in each histological section, averaged over all sections containing that plaque type across all pigs. The final readout was then scaled by the maximum WSS metric value across all metrics analysed to facilitate comparisons between metrics.

Error analysis

To quantify the resolution of our output metrics (e.g., WSS), we performed an error analysis on the primary components that make up the workflow of our system, including the accuracy of FD-OCT, 3-D histology, and characterizing plaque morphology locally within each cross-section.

FD-OCT has a resolution of 15 μm in-plane and 200 μm axially (referring to the long-axis of the vessel, which is sometimes also called the longitudinal direction). This results in an in-plane error of 0.9% for an average pig vessel radius of 1.75 mm. Because FD-OCT cannot be gated, an additional error is introduced due to motion of the vessel over the cardiac cycle. The diameter change of the vessel during the cardiac cycle was measured by recording an intravascular ultrasound (IVUS) measurement without pulling back for one vessel in one pig. We introduced pump injection of iodinated contrast during this IVUS measurement to simulate the pressure experienced by the vessel during normal FD-OCT pullback, which might attenuate vessel motion over the cardiac cycle. We found fluctuations of 1 mm^2 around an average area of 16.5 mm^2, which corresponds to an error in the radius of 3%. The overall combined error, therefore, in reconstructing vessel radius is 3.1% or 54 μm, which equates to an error in WSS of 9.3% (because WSS is dependent on the cube of the radius). As IVUS

was used, which has an in-plane resolution of 200 μm, the computed error represents the maximum error expected in our FD-OCT based reconstructions. Nevertheless, an error in WSS of less than 10% compares favourably with previous reports from both our[16, 18, 19] and other groups[20-24].

Next, the error associated with co-registration of the histology information onto the vessel reconstruction was assessed. We computed error as the difference in observations and measurements of these steps from the same observer at two time points, 6 months apart and in a masked fashion the second time. In the axial direction, error was due to the axial increment of obtaining histological sections, identification of matches between FD-OCT frames and histology sections, and measurements of the vessel at different stages of histological processing. For these three processes, the average error over all instrumented vessels was found to be ~105 μm, 280±111 μm and 162±61 μm, respectively, which equates to a combined error of 340 μm. Thus, this axial error is within the resolution of 2 FD-OCT frames. Circumferentially, the error was due to identification of the myocardium on the reconstructed vessel based on qualitative examination of the largest inner curvature. Over all reconstructed instrumented vessels at all time points, this error was found to be 11.4±3.6°, which is equivalent to an arc length of 265±82 μm.

Finally, the error in characterizing plaque morphology was assessed by having the same observer re-classify plaque types on 20 sections selected from all vessel locations and pigs 3 months after the original classification and in a masked fashion the second time. The average error was 8.9% over all sections. Inconsistencies were found only in the classification of early lesions (XA and IT) and normal vessel wall (NOR), whereas all advanced plaque types were re-classified exactly the same as the original classification.

Supplemental Tables

Supplemental Table 1: Summary of WSS metrics of disturbed flow used in this study and the mathematical formulation for each.

Hemodynamic Parameter	Formulation
Time Averaged Wall Shear Stress (WSS)	$WSS = \frac{1}{T}\int_0^T \lvert\vec{\tau}_w\rvert\, dt$
WSS gradient (SG)	$\mathrm{SG} = \frac{1}{T}\int_0^T \sqrt{\left(\frac{\partial\vec{\tau}_w}{\partial x}\right)^2 + \left(\frac{\partial\vec{\tau}_w}{\partial y}\right)^2 + \left(\frac{\partial\vec{\tau}_w}{\partial z}\right)^2}\, dt$
WSS Angle Deviation (SAD)	See Hyun et al.[13]
Oscillatory Shear Index (OSI)	$OSI = \frac{1}{2}\left[1 - \frac{\left\lvert\int_0^T \vec{\tau}_w\, dt\right\rvert}{\int_0^T \lvert\vec{\tau}_w\rvert\, dt}\right]$
Relative Residence Time (RRT)	$RRT \sim \frac{1}{(1 - 2\cdot OSI)\cdot WSS}$
Low Shear Index (LSI)	$LSI = \frac{(WSS_{Threshold} - WSS_{SMS})}{WSS_{Threshold}}$ $WSS_{Th} = \exp\left(mean\left(ln(WSS_{Base})\right) - 1.28\cdot SD\left(ln(WSS_{Base})\right)\right)$
High Shear Index (HSI)	$HSI = \frac{(WSS_{SMS} - WSS_{Threshold})}{WSS_{SMS}}$ $WSS_{Th} = \exp\left(mean\left(ln(WSS_{Base})\right) + 1.28\cdot SD\left(ln(WSS_{Base})\right)\right)$
Transverse Wall Shear Stress (tSS)	$tSS = \frac{1}{T}\int_0^T \left\lvert\vec{\tau}_w.\left(\vec{n}\times\frac{\int_0^T \vec{\tau}_w\, dt}{\left\lvert\int_0^T \vec{\tau}_w\, dt\right\rvert}\right)\right\rvert\, dt$ $\vec{n}$ represents the normal to the arterial surface

Supplemental Figures and Figure Legends

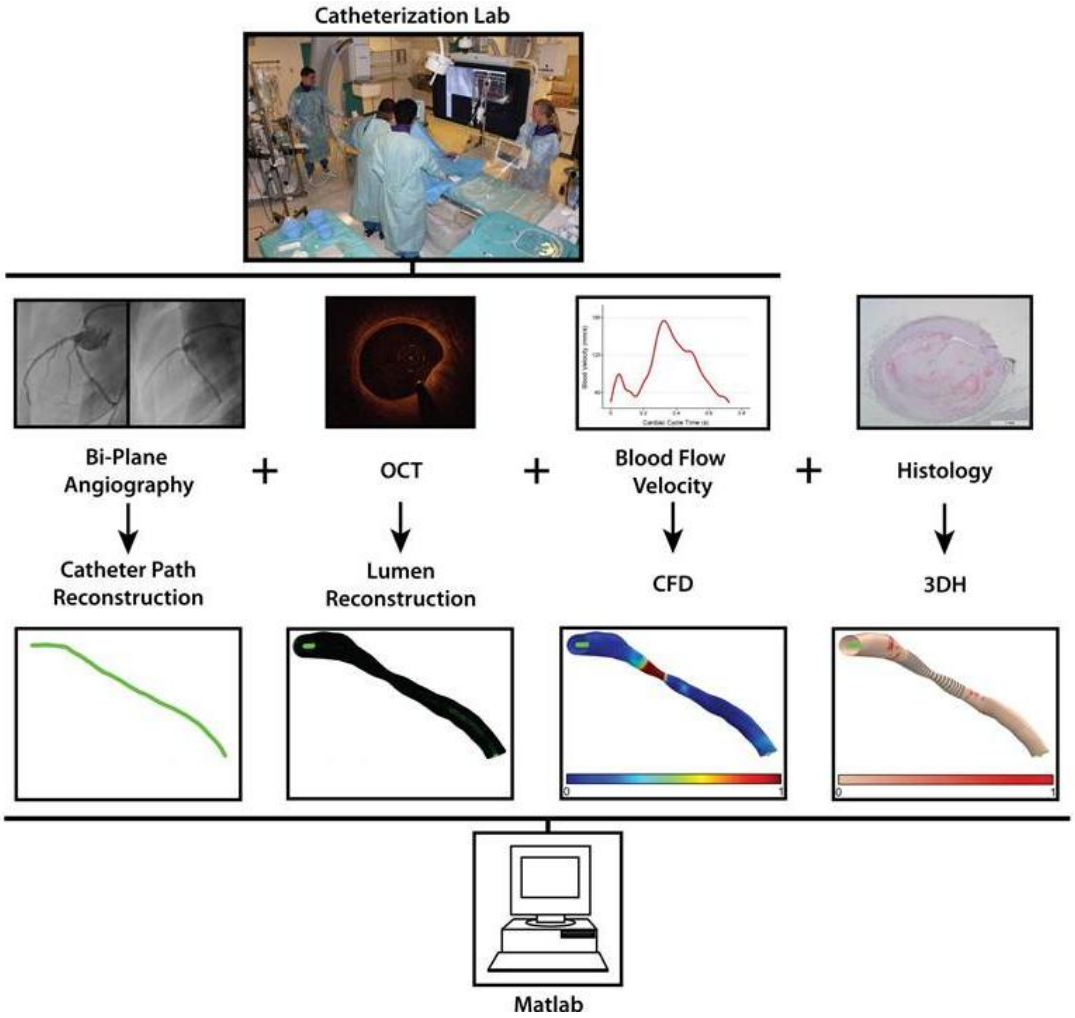

Supplemental Figure 1. Workflow of the data acquired during cardiac catheterization and downstream analysis. For each vessel at each time point, bi-plane angiography of the FD-OCT catheter path is performed immediately before pullback. The FD-OCT pullback is performed, acquiring image cross-sections over a vessel length of ~50 mm. Finally, blood velocity measurements were acquired at the inlet of each vessel using a Combowire. These measurements allowed reconstruction of the catheter path and vessel lumen to perform CFD, which, in turn, allowed calculation of WSS metrics of disturbed flow. Histological data were co-registered to the vessel reconstructions and thus WSS metrics to investigate whether any plaque types co-localized with particular flow disturbances. Most of these analysis steps employed custom Matlab software developed in-house, as described above.

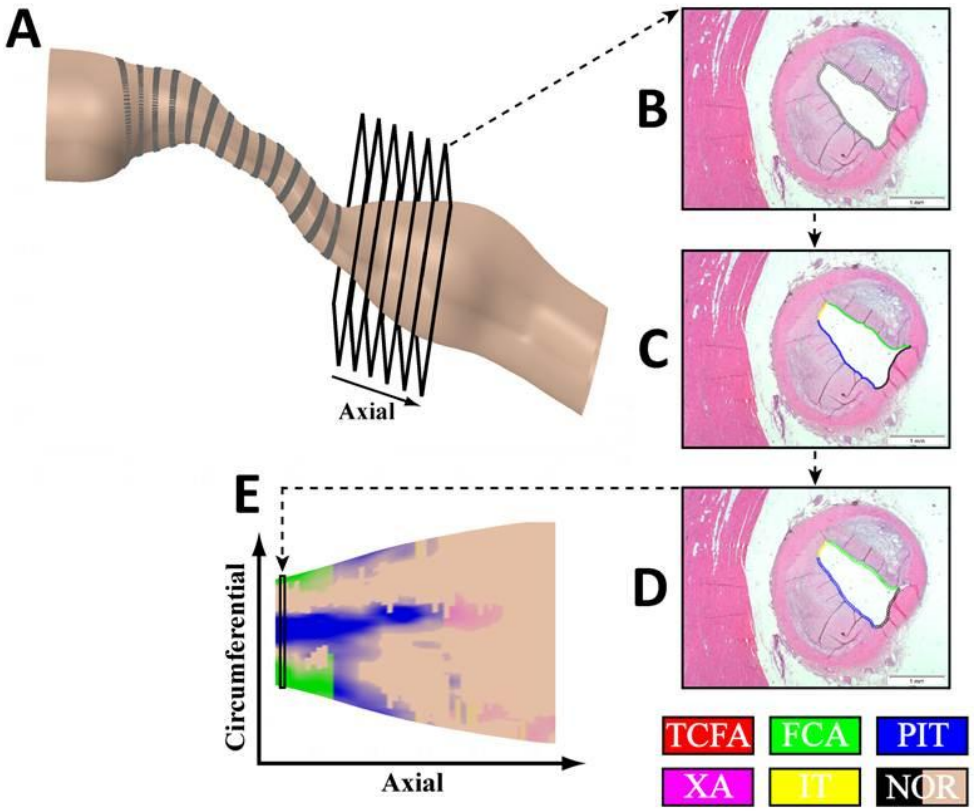

Supplemental Figure 2. Processing steps taken to characterize plaque type from H&E stained histology sections and co-register it to the *in vivo* lumen reconstruction from FD-OCT. (A) The reconstructed vessel post-implantation of the stent (shown in grey) and the location from which serial sections were acquired downstream of the stent (sections acquired upstream are not indicated). (B) Each section is manually segmented and the contour is discretized into a user-defined number of nodes by custom software. (C) Colored lines are manually drawn around the lumen of each section to indicate plaque type (TCFA – red, FCA – green, PIT – blue, XA – violet, IT – yellow, and NOR – black or beige). (D) Custom software is used to extract the color from the image and store it within the corresponding nodes of the reconstructed lumen contour. (E) The nodes of the histology lumen are co-registered to the reconstructed *in vivo* lumen segment (from which they were derived), which can be isolated and laid flat (endothelium upwards) to display the pattern of each plaque type. After co-registration, each node of the reconstructed lumen (and histology sections) has plaque type and all WSS metrics defined.

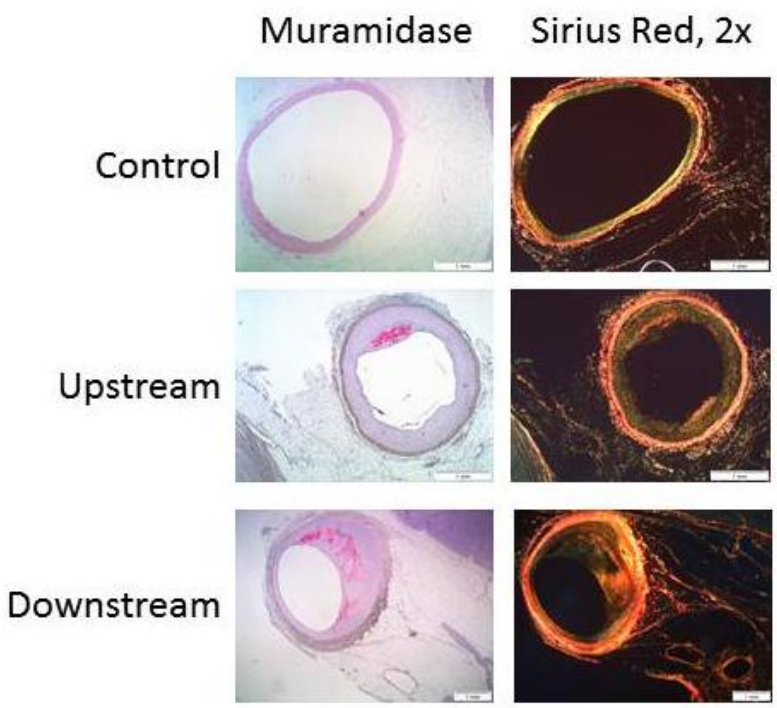

Supplemental Figure 3. Representative images of histological sections stained for macrophages (muramidase) and collagen (picrosirius red) in the control and upstream and downstream SMS vessel segments, demonstrating larger plaques in the downstream SMS segment.

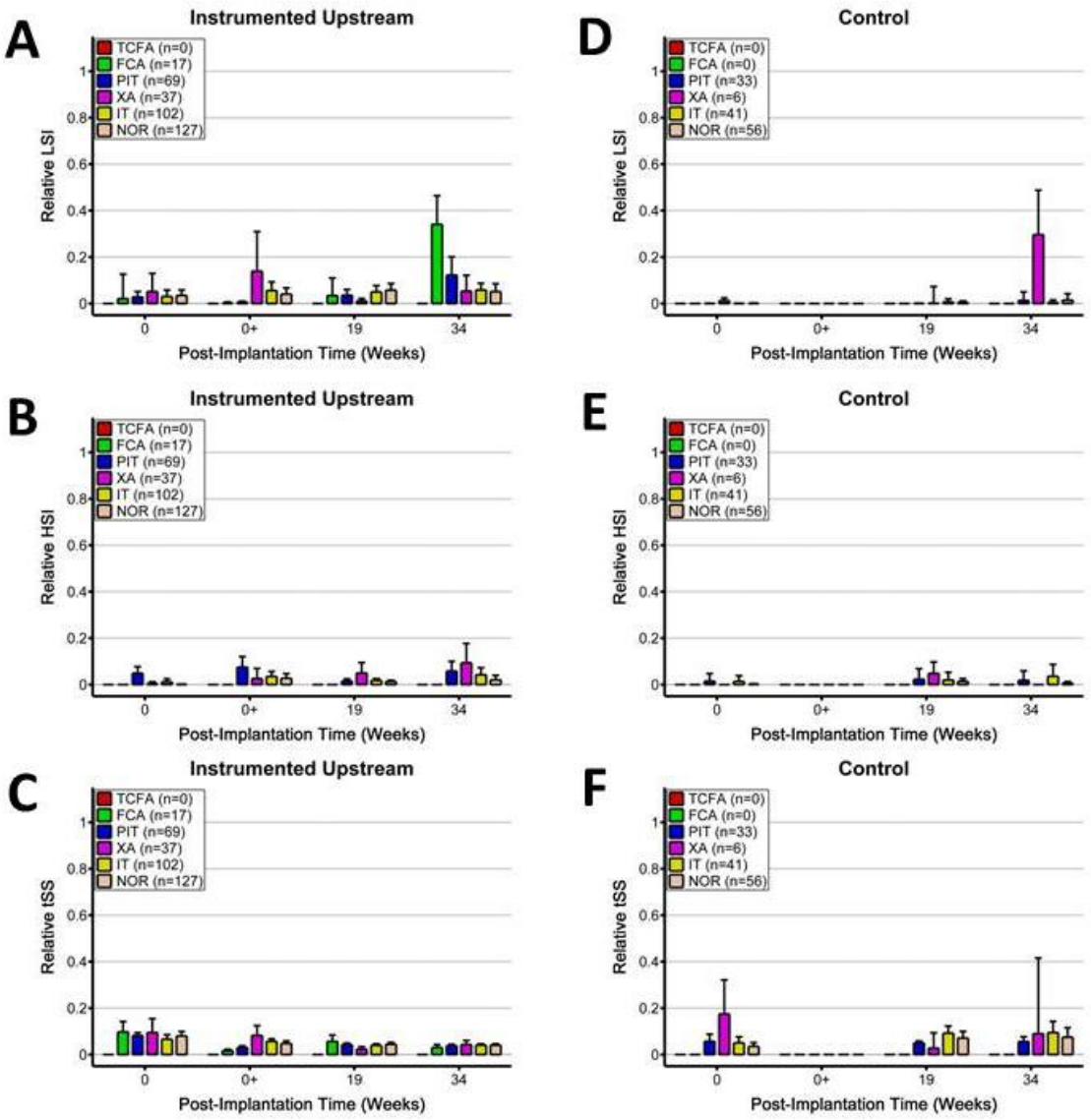

Supplemental Figure 4. LSI, HSI, and tSS within each plaque type of the instrumented downstream segment, averaged over all sections containing that plaque type and all pigs at each time point. All shear values are scaled by the maximum over all shear metrics (LSI at 19 weeks in the downstream instrumented vessel, seen in Figure 5A) to facilitate comparisons. Panels A, B, C show each metric, respectively, in the instrumented upstream segment and panels D, E, F similarly show each metric in the control segment. These plots demonstrate a relative absence of these metrics of disturbed flow in these vessel segments and, over all times as a whole, there were no statistical differences between these metrics in progressive lesions versus other plaque types. Individual plaque comparisons at each time point were not considered. Data are expressed as geometric mean plus upper limit of 95%CI.

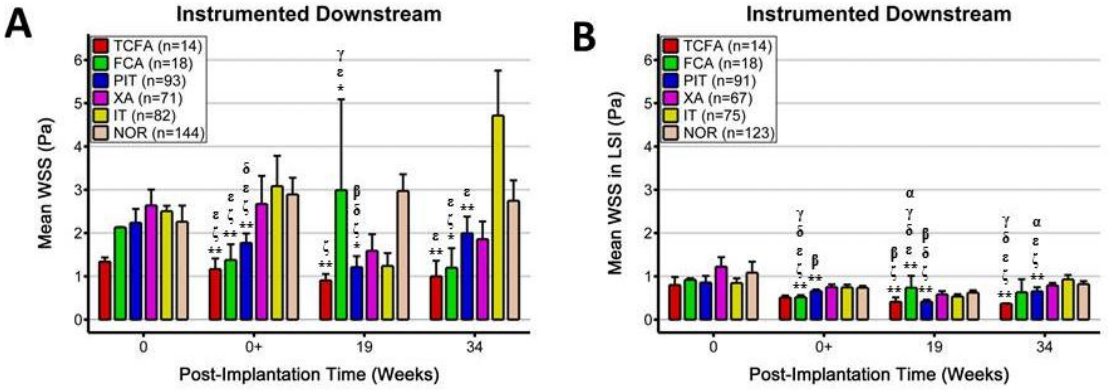

Supplemental Figure 5. (A) Absolute values of WSS averaged over all regions of each plaque type. Over all times as a whole, there were no statistical differences between the advanced plaque types. TCFA and PIT were statistically different from both IT (p<0.005) and normal wall (p<0.005), but FCA was statistically different from normal wall only (p<0.005). This finding demonstrates that LSI and HSI better distinguish between plaque types, based on magnitude changes of WSS in diseased compared to normal or baseline vessels, compared to WSS alone. (B) Absolute values of WSS averaged only within regions of each plaque type that contain LSI values greater than zero. Over all times as a whole, TCFA was statistically different from FCA (p<0.005), as well as XA (p=0.048) and normal wall (p<0.005). PIT exhibited the only other statistical difference, compared to normal wall (p<0.005). The geometric mean of these values is 0.7 [0.6, 0.8] Pa, averaged over all plaque types and time points (including baseline). This finding demonstrates a potential improvement to previous investigators who used a much higher binary threshold (1 – 1.2 Pa) to determine low shear, which may not be as specific to regions of plaque development. *Indicates statistically different values of WSS within the plaque type designated by the bar over which it is placed versus other plaque types (TCFA – α, FCA – β, PIT – γ, XA – δ, IT – ε, and NOR – ζ). Data are expressed as geometric mean plus upper limit of 95%CI.

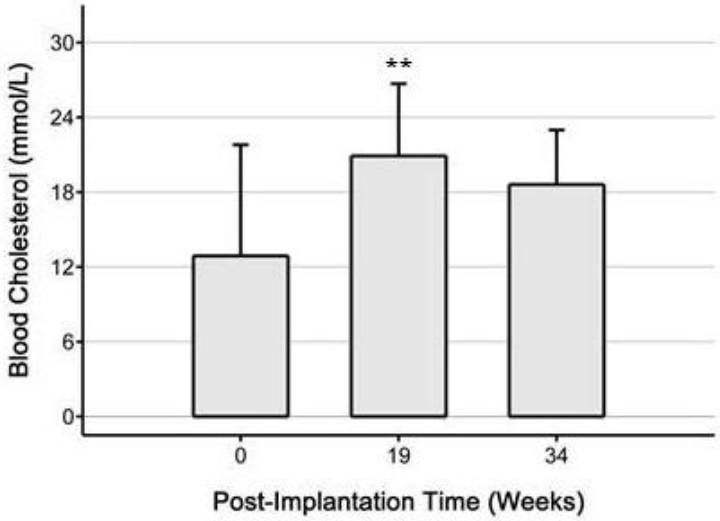

Supplemental Figure 6. Total blood cholesterol levels (mmol/L) averaged over all pigs at each time point. Compared to baseline, there was a statistically significant increase at 19 weeks (**p=0.006), which reduced at 34 weeks and was not significantly different from baseline (p=0.082). The threshold for abnormally elevated blood cholesterol is ~2 mmol/L (~77 mg/dl). Data are expressed as mean±SD.

Supplemental References

1. Al-Mashhadi RH, Sorensen CB, Kragh PM, Christoffersen C, Mortensen MB, Tolbod LP, Thim T, Du Y, Li J, Liu Y, Moldt B, Schmidt M, Vajta G, Larsen T, Purup S, Bolund L, Nielsen LB, Callesen H, Falk E, Mikkelsen JG, Bentzon JF. Familial hypercholesterolemia and atherosclerosis in cloned minipigs created by DNA transposition of a human pcsk9 gain-of-function mutant. *Sci Transl Med*. 2013;5:166ra161
2. Foin N, Sen S, Petraco R, Nijjer S, Torii R, Kousera C, Broyd C, Mehta V, Xu Y, Mayet J, Hughes A, Di Mario C, Krams R, Francis D, Davies J. Method for percutaneously introducing, and removing, anatomical stenosis of predetermined severity in vivo: The "stenotic stent". *J Cardiovasc Transl Res*. 2013;6:640-648
3. Falk E, Fallon JT, Mailhac A, Fernandezortiz A, Meyer BJ, Weng D, Shah PK, Badimon JJ, Fuster V. Muramidase - a useful monocyte/macrophage immunocytochemical marker in swine, of special interest in experimental cardiovascular-disease. *Cardiovasc Pathol*. 1994;3:183-189
4. Wahle A, Prause PM, DeJong SC, Sonka M. Geometrically correct 3-d reconstruction of intravascular ultrasound images by fusion with biplane angiography--methods and validation. *IEEE transactions on medical imaging*. 1999;18:686-699
5. Post AL, Poulsen CB, Pedrigi RM, Mehta V, Pareek N, Foin N, Holm NR, Davies J, Andersen HR, Bøtker HE, Bjørklund MM, Andersen NP, Grøndal AK, Di Mario C, Falk E, Krams R, de Silva R. Lowering shear stress in hypercholesterolaemic pig arteries may accelerate atherosclerotic plaque formation. *The 8th international symposium on Biomechanics in Vascular Biology and Cardiovascular Disease*. 2013
6. Trachet B, Renard M, De Santis G, Staelens S, De Backer J, Antiga L, Loeys B, Segers P. An integrated framework to quantitatively link mouse-specific hemodynamics to aneurysm formation in angiotensin ii-infused apoe -/- mice. *Annals of biomedical engineering*. 2011;39:2430-2444
7. Valentin A, Humphrey JD, Holzapfel GA. A finite element-based constrained mixture implementation for arterial growth, remodeling, and adaptation: Theory and numerical verification. *International journal for numerical methods in biomedical engineering*. 2013;29:822-849
8. Timmins LH, Molony DS, Eshtehardi P, McDaniel MC, Oshinski JN, Samady H, Giddens DP. Focal association between wall shear stress and clinical coronary artery disease progression. *Annals of biomedical engineering*. 2015;43:94-106
9. Rikhtegar F, Knight JA, Olgac U, Saur SC, Poulikakos D, Marshall W, Jr., Cattin PC, Alkadhi H, Kurtcuoglu V. Choosing the optimal wall shear parameter for the prediction of plaque location-a patient-specific computational study in human left coronary arteries. *Atherosclerosis*. 2012;221:432-437
10. Ku DN, Giddens DP, Zarins CK, Glagov S. Pulsatile flow and atherosclerosis in the human carotid bifurcation. Positive correlation between plaque location and low oscillating shear stress. *Arteriosclerosis*. 1985;5:293-302
11. He X, Ku DN. Pulsatile flow in the human left coronary artery bifurcation: Average conditions. *Journal of biomechanical engineering*. 1996;118:74-82
12. Himburg HA, Grzybowski DM, Hazel AL, LaMack JA, Li XM, Friedman MH. Spatial comparison between wall shear stress measures and porcine arterial endothelial permeability. *American journal of physiology. Heart and circulatory physiology*. 2004;286:H1916-1922
13. Hyun S, Kleinstreuer C, Archie JP, Jr. Hemodynamics analyses of arterial expansions with implications to thrombosis and restenosis. *Medical engineering & physics*. 2000;22:13-27
14. Peiffer V, Sherwin SJ, Weinberg PD. Computation in the rabbit aorta of a new metric - the transverse wall shear stress - to quantify the multidirectional character of disturbed blood flow. *J Biomech*. 2013;46:2651-2658

15. Peiffer V, Sherwin SJ, Weinberg PD. Does low and oscillatory wall shear stress correlate spatially with early atherosclerosis? A systematic review. *Cardiovascular research*. 2013;99:242-250
16. Segers D, Helderman F, Cheng C, van Damme LC, Tempel D, Boersma E, Serruys PW, de Crom R, van der Steen AF, Holvoet P, Krams R. Gelatinolytic activity in atherosclerotic plaques is highly localized and is associated with both macrophages and smooth muscle cells in vivo. *Circulation*. 2007;115:609-616
17. Virmani R, Kolodgie FD, Burke AP, Farb A, Schwartz SM. Lessons from sudden coronary death: A comprehensive morphological classification scheme for atherosclerotic lesions. *Arterioscler Thromb Vasc Biol*. 2000;20:1262-1275
18. Krams R, Cheng C, Helderman F, Verheye S, van Damme LC, Mousavi Gourabi B, Tempel D, Segers D, de Feyter P, Pasterkamp G, De Klein D, de Crom R, van der Steen AF, Serruys PW. Shear stress is associated with markers of plaque vulnerability and mmp-9 activity. *EuroIntervention*. 2006;2:250-256
19. Krams R, Verheye S, van Damme LC, Tempel D, Mousavi Gourabi B, Boersma E, Kockx MM, Knaapen MW, Strijder C, van Langenhove G, Pasterkamp G, van der Steen AF, Serruys PW. In vivo temperature heterogeneity is associated with plaque regions of increased mmp-9 activity. *European heart journal*. 2005;26:2200-2205
20. Chatzizisis YS, Baker AB, Sukhova GK, Koskinas KC, Papafaklis MI, Beigel R, Jonas M, Coskun AU, Stone BV, Maynard C, Shi GP, Libby P, Feldman CL, Edelman ER, Stone PH. Augmented expression and activity of extracellular matrix-degrading enzymes in regions of low endothelial shear stress colocalize with coronary atheromata with thin fibrous caps in pigs. *Circulation*. 2011;123:621-630
21. Chatzizisis YS, Jonas M, Coskun AU, Beigel R, Stone BV, Maynard C, Gerrity RG, Daley W, Rogers C, Edelman ER, Feldman CL, Stone PH. Prediction of the localization of high-risk coronary atherosclerotic plaques on the basis of low endothelial shear stress: An intravascular ultrasound and histopathology natural history study. *Circulation*. 2008;117:993-1002
22. Koskinas KC, Feldman CL, Chatzizisis YS, Coskun AU, Jonas M, Maynard C, Baker AB, Papafaklis MI, Edelman ER, Stone PH. Natural history of experimental coronary atherosclerosis and vascular remodeling in relation to endothelial shear stress: A serial, in vivo intravascular ultrasound study. *Circulation*. 2010;121:2092-2101
23. Koskinas KC, Sukhova GK, Baker AB, Papafaklis MI, Chatzizisis YS, Coskun AU, Quillard T, Jonas M, Maynard C, Antoniadis AP, Shi GP, Libby P, Edelman ER, Feldman CL, Stone PH. Thin-capped atheromata with reduced collagen content in pigs develop in coronary arterial regions exposed to persistently low endothelial shear stress. *Arteriosclerosis, thrombosis, and vascular biology*. 2013;33:1494-1504
24. Wentzel JJ, Whelan DM, van der Giessen WJ, van Beusekom HM, Andhyiswara I, Serruys PW, Slager CJ, Krams R. Coronary stent implantation changes 3-d vessel geometry and 3-d shear stress distribution. *Journal of biomechanics*. 2000;33:1287-1295

Inducing Persistent Flow Disturbances Accelerates Atherogenesis and Promotes Thin Cap Fibroatheroma Development in *D374Y*-PCSK9 Hypercholesterolemic Minipigs

Ryan M. Pedrigi, Christian Bo Poulsen, Vikram V. Mehta, Niels Ramsing Holm, Nilesh Pareek, Anouk L. Post, Ismail Dogu Kilic, Winston A.S. Banya, Gianni Dall'Ara, Alessio Mattesini, Martin M. Bjørklund, Niels P. Andersen, Anna K. Grøndal, Enrico Petretto, Nicolas Foin, Justin E. Davies, Carlo Di Mario, Jacob Fog Bentzon, Hans Erik Bøtker, Erling Falk, Rob Krams and Ranil de Silva

Circulation. published online July 15, 2015;
Circulation is published by the American Heart Association, 7272 Greenville Avenue, Dallas, TX 75231

Print ISSN: 0009-7322. Online ISSN: 1524-4539